Wireless Embedded System with Applications to Renewable Energy and Energy Efficiency

by

Younes Rashidi

B.Sc., Shiraz University, 1993

THESIS SUBMITTED IN PARTIAL FULFILLMENT
OF THE REQUIREMENTS FOR THE DEGREE OF

MASTER OF APPLIED SCIENCE

in the
Mechatronic Systems Engineering, School of Engineering Science
Faculty of Applied Science

SIMON FRASER UNIVERSITY

Summer 2012

Approval

Name: **Younes Rashidi**

Degree: **Master of Applied Science (Mechatronic Systems Engineering)**

Title of Thesis: **Wireless Embedded System with Applications to Renewable Energy and Energy Efficiency**

Examining Committee:

Chair: **Dr. Krishna Vijayaraghavan**, Assistant Professor of Engineering Science

---

Dr. Mehrdad Moallem
Senior Supervisor
Associate Professor of Engineering Science

Dr. Ahmad Rad
Supervisor
Professor of Engineering Science

Dr. Craig Scratchley
Internal Examiner
Senior Lecturer of Engineering Science

Date Defended/Approved: May 7, 2012

Partial Copyright Licence

Abstract

Renewable sources of energy are considered as viable alternatives to cope with environmental issues related to non-renewable energies and the energy crisis of the current century. However, there are certain challenges in the production and consumption of renewable sources of energy. In this thesis, we study the problem of monitoring power production in photovoltaic (PV) solar energy systems and energy-efficient lighting control through wireless embedded microcontroller systems. In particular, two applications in energy production and conservation are studied. First, a ZigBee-enabled solar PV power performance monitoring system at the module level is developed that enables the user to reduce operation and maintenance costs through real-time monitoring of power production. Due to the relatively high cost of solar energy production, Light Emitting Diode (LED) lighting is a natural choice to reduce energy consumption for lighting. Thus, an energy-efficient LED testbed is developed using the Bluetooth low energy (BLE) wireless technology. To this end, two lab prototypes are developed and implemented for both applications, and their performance is tested through experiments. Furthermore, a graphical user interface (GUI), is developed that can be utilized for monitoring and supervisory control purposes related to the testbeds developed in this work.

Keywords: Renewable energy; Energy efficiency; Photovoltaic solar; Wireless embedded system; ZigBee; Bluetooth low energy

To my lovely wife and children

Acknowledgements

I would like to express my profound gratitude to my supervisor, Dr. Mehrdad Moallem, for his guidance and support, as well as all his endeavors in running such an energetic research lab. My appreciation also goes to my lab mates for their understanding during the times we spent together.

Last, but most importantly, I would like thank my family and dedicate this thesis to them for their encouragement and patience during my years of research that have made this work possible.

Table of Contents

List of Tables

List of Figures

List of Acronyms

ACL	Access Control List
AP	Wireless Access Point
BAN	Body Area Network
BLE	Bluetooth Low Energy
BPSK	Binary phase-shift keying
BSS	Basic Service Set
CSMA-CA	Carrier Sense Multiple Access with Collision Avoidance
DFS	Dynamic Frequency Selection
DS	Distribution System
ESS	Extended Service Set
FDMA	Frequency Division Multiple Access
FHSS	Frequency Hopping Spread Spectrum
GFSK	Gaussian Frequency-Shift Keying
HAN	Home Area Network
HCI	Hardware Controller Interface
IBSS	Independent Basic Service Set
ISM	Industrial, Scientific and Medical
L2CAP	Logical Link Control and Adaptation Protocol
LLC	Logical Link Control
MAC	Media Access Control
MIMO	Multiple-Input-Multiple-Output
OQPSK	Offset Quadrature Phase-Shift Keying
PAN	Personal Area Network
PHY	Physical
PV	Photovoltaic
QoS	Quality of Service
STA	Station
TDMA	Time Division Multiple Access
TPC	Transmit Power Control
UART	Universal Asynchronous Receiver and Transmitter
UWB	Ultra-Wideband

WLAN	Wireless Local Area Network
WSN	Wireless Sensor Network

Chapter 1: Introduction

Energy plays a pivotal role in human life. The sun was the very first energy source that man used for lighting and heating purposes. Later, humans uncovered other energy sources such as water and wind, and learned to employ them to improve their living conditions. For thousands of years, people have continued to discover and harness more energy sources from nature and utilize them in order to facilitate human advancement. However, as human societies steadily grew and energy demand increased, an entirely new set of challenges arose, involving energy supply production and conservation. Modern society endeavored to respond to these challenges through a number of innovative techniques and strategies. Progress led to the production of alternative energy and a shift in the manner of consumption. For instance, electricity was generated by harnessing the energy of water, and distribution systems, along with energy storing technologies, were created in order to fulfil growing energy needs.

Although many of the energy concerns have been resolved during previous centuries, there exists serious anxiety about environmental implications of using non-renewable energy sources such as oil, coal, and uranium. Moreover, the non-renewable sources are a main contributor of energy resources, and they are being consumed much faster than is in nature's capacity to reproduce them. For example, oil was generated in the earth over the course of hundreds of millions of years, and considering oil production of around 91.1 million barrels per day[1], it will run out in hundreds of years. Additionally, non-renewable energies produce an adverse impact on the environment and contribute to climate change and global warming. In contrast, renewable energies such as solar, tidal, biomass and wind are sustainable energy resources presenting environmentally

[1] Source: International Energy Agency (IEA) Oil market report on June 2012, http://omrpublic.iea.org/currentissues/full.pdf.

friendly features. They are crucial in the move towards the future world of energy, and a myriad of countries have planned to obtain their energy needs via renewable sources. Europe, for instance, has committed to obtaining 20% of its energy from renewable sources by 2020[2]. However, efficiency and economic issues are some of the main challenges of renewable energies [1]. The conversion efficiency of a typical photovoltaic (PV) solar cell, for example, is about 21%, which means much of the energy from sunlight reaching a PV cell (i.e., approximately 79%) is lost before it can be converted into electricity [2]. Table 1.1 illustrates the levelized cost of electricity (LCOE)[3] for several different energy resources [3]. It clearly shows that the electricity production cost for the solar PV is double the amount of non-renewable energy resources such as conventional coal. Although the wind power LCOE is not a significant concern, it has a serious drawback of requiring large land areas to produce useful amounts of heat or electricity [4].

Table 1.1: The estimated cost of electricity for several different energy sources

Energy Plant Type	LCOE ¢ per kWh
Natural Gas	6.4
Conventional Coal	7.5
Wind power	8.4
Advanced Nuclear	10.0
Solar PV	15.0
Solar Thermal	16.0

From an environmental perspective, solar power is the most abstract and attainable alternative renewable source of energy [5] that has motivated scientists to conduct research into this area regarding cost, performance, and efficiency. Referring to the LCOE formula, one of the possibilities for decreasing the production cost of solar power is the reduction of the total life cycle cost (TLCC). Operating and maintenance costs of a system significantly affect TLCC and consequently are noteworthy and

[2] Source: European Environment Agency (EEA)

[3] $LCOE = \frac{Total\ Life\ Cycle\ Cost}{Total\ Lifetime\ Energy\ Production}$

attractive areas for researchers to devise novel mechanisms in order to reduce the LCOE of solar power. Considering small-scale local power generation and employing a strategy for reducing consumption is another approach to coping with the economic challenges of solar power. This strategy has spun new research areas such as net-zero energy buildings [6] and energy-efficient buildings [7]. This thesis focuses on two case studies to address certain problems related to the above topics. In particular, we study how to reduce the cost of solar power production through not only reducing operating and maintenance costs but also reviewing a technique in order to decrease energy demand.

Achieving these goals requires the use of an automated control and monitoring system to manage power production and consumption. This objective can be achieved by developing an embedded computer system that is able to communicate with a control and monitoring module acting as a host computer. An embedded system is a programmable computer that takes advantage of the application in its design to perform specific control functions [8]. Depending on the application, it interfaces with other parts of a system through wired, or wireless, communication. Wireless-enabled embedded systems are utilized in this research to develop the control and monitoring system for performance monitoring in solar power production as well as developing an energy-efficient system in buildings that can be used for lighting and other applications such as heating, ventilation, and air conditioning (HVAC).

1.1. Solar PV Power, Economic Issues, and Solutions

Every day, the sun delivers a vast amount of energy to the earth, free of charge. The average intensity of solar radiation on the earth orbit is 1367kW/m^2, and the earth's equatorial circumference is 40,000km, hence the earth acquires up to 173,000TW of energy from the sun [9]. This energy is available everywhere, and it can be used for different purposes (e.g. producing electricity or water heating). Several technologies can convert solar energy into electricity, such as concentrating solar power (CSP) and solar photovoltaic (PV) devices. In solar photovoltaic, the sun’s radiation is directly converted into electricity by solar cells that are made of semiconductor materials. When sunlight radiates onto these materials, it causes free electrons to be generated in the conduction

bands of the semiconductor crystalline, which is equivalent to producing electricity [9]. Considering the vast potential of solar energy, PV is poised to become a major resource of clean electricity in the future.

In a typical photovoltaic system, several modules (see Figure 1.1) are connected to form module strings. For larger PV systems, several of these strings are connected in parallel. Certain de-rating factors such as aging, shadowing, manufacturing mismatch, and wiring or inverter losses are accounted for in designing a PV system. However, other factors such as unforeseen temporary shading and uneven soiling or system defects developed after installation can cause total system shut down in certain cases that are not foreseeable at the design stage. A PV string can easily lose a significant portion of its total output with only a partially underperforming single module [10]. In the worst-case scenario, where many modules are bypassed, the string voltage can fall below the minimum recommended input DC voltage specified for the inverter, causing a significant drop in the inverter efficiency or complete inverter shutdown. The system's down-time involves informing the maintenance crew and locating underperforming modules, as well as a rapid response to remedy or replace them, which are time-consuming tasks. This amount of system down-time, especially on the utility-scale, increases total life cycle costs, and consequently raises the levelized cost of electricity (LCOE) for solar PV systems. The above problem may be alleviated by monitoring a PV system at the module level, so that any drop in PV system performance can be immediately traced to the module causing the problem [11]. This feature, if implemented at the PV module stage, can remarkably reduce the system down-time. Hence, in the long-term usage of the PV module, it can significantly decrease the operation and maintenance costs, leading to a lower LCOE of solar PV power. Although several factors affect LCOE, the cost of operation and maintenance is a principal contributor that has motivated us to pursue this line of research.

Figure 1.1: A typical series string of PV modules.

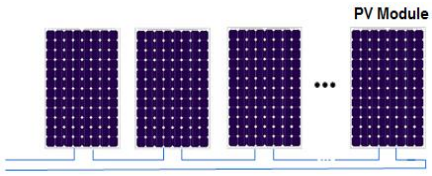

To implement a PV module monitoring system at the module level, module level voltage and current sensing are required in the form of a hardware unit that can be inserted into the junction box of each PV panel. However, this hardware requires communication with a central station to report the status of the PV module. To this end, a promising candidate that can offer a cost-effective communication system is modern wireless technology. A wireless-enabled embedded system can offer local processing (e.g. voltage and current sensing) and communication needs. There exist several wireless technologies to be utilized as an appropriate candidate for PV module monitoring, as discussed in Chapter 2.

1.2. Electric Power Demand and Energy-Efficient Systems in Buildings

Transportation, manufacturing, heating, cooling, lighting, and many other needs in modern society rely on electricity. The consumption factors that determine electric power demand differ in geography, climate, and application types. Regardless of these factors, buildings are one of the main contributors to energy consumption which should be considered in energy-efficient systems. Achieving energy conservation in buildings depends on how well the demand is managed while meeting requirements such as occupant comfort, health, and safety. Figure 1.2 demonstrates the energy consumption breakdown in commercial buildings, indicating that 70% of the total energy is consumed by lighting and HVAC systems. Indeed, 38% of the total energy in a commercial building is used for lighting, which is undoubtedly a principal contributor to electric power consumption. This fact has motivated researchers and developers to seek techniques for reducing energy demand for lighting applications in buildings. Some studies suggest the replacement of older fixtures with new luminaries to improve efficiency [12], while some others recommend utilizing an occupancy detector for performing an automatic switch to turn the light OFF when it is no longer necessary [13]. Although all these methods are realistic, the amount of electric power conservation depends on technologies and applied techniques.

Figure 1.2: Energy consumption breakdown in commercial buildings.

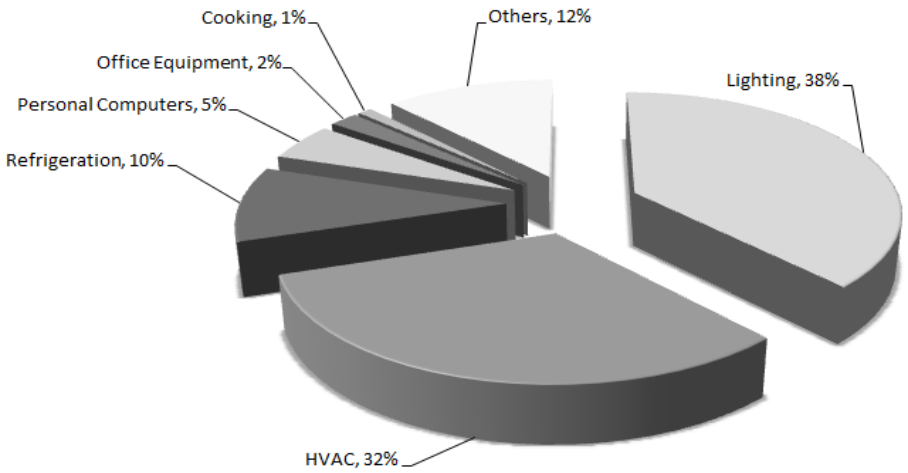

[Source: U.S. Energy Information Administration (EIA)]

Among efficient lighting technologies, fluorescent and compact fluorescent lamps (CFL) have been employed for several decades to replace inefficient incandescent lighting lamps. However, there is a great potential for energy efficiency using new technologies and control mechanisms. For example, solid-state lighting technology has been newly introduced in the form of state-of-the-art LED lighting solutions with higher luminous efficacy in comparison with incandescent, florescent or CFL lighting, albeit with lower power consumption [14]. The LED is controllable using DC current drive and allows for a dimming mechanism and daylight harvesting. These features, combined with an intelligent controller, have the capacity to achieve highly efficient lighting solutions for buildings. Although such a system in new buildings can be considered in the design phase, retrofitting current lighting systems is a challenging task due to the amount of the wiring involved. Short-range wireless technologies are well-known solutions for wiring replacement that are widely employed in building applications. However, robustness, reliability, and power drive are some of the main concerns in wireless applications that motivated researchers into these subjects. The second part of the proposed research (see Chapter 4) utilizes newly introduced wireless connectivity, featuring ultra-low power consumption technology in order to design and implement an energy-efficient lighting system using LED lighting technology.

1.3. Thesis Organization

The rest of this thesis is organized as follows. In Chapter 2, we address several different wireless technologies including local area networks (LANs) and personal area networks (PANs) that are potential candidates for employment in renewable energy and energy efficiency applications. Considering a wide range of brand-based features that are added to wireless technologies, all data and tables in this chapter are extracted from the most reliable references (e.g., IEEE 802.11 standard for Wi-Fi technology). Chapter 3 presents the design of an embedded wireless system for installation on a PV module and its user interface that can perform current, voltage, and power monitoring system using the ZigBee wireless technology. A proof-of-concept system is built and experimental results are discussed in this chapter. In Chapter 4, Bluetooth low energy technology is utilized to design, implement, and develop an energy-efficient LED lighting system. A testbed is developed for a proof-of-concept 150W LED lighting system. Chapter 5 provides concluding remarks and directions for future research.

Chapter 2: Wireless Embedded Systems

Nowadays, wireless technologies have widely permeated all aspects of human life. Personal area network (PAN) [15] and wireless body area network (WBAN) [16] are some examples of short-range wireless applications. However, the diversity of usage cases has created a variety of wireless standards such as Z-wave, Wi-Fi, and Bluetooth [17]-[18]. Table 2.1 illustrates a comparison between several well-known wireless technologies: Wi-Fi [19], Bluetooth [20], Bluetooth low energy (BLE) [20], ZigBee [21], Z-Wave [22], and ANT+ [23]. Although each standard has several versions (e.g. Wi-Fi has IEEE 802.11a, b, g, and n), the most popular types are considered for this comparison. Wi-Fi is mainly applicable in wireless local area networks (WLAN), and provides secure connectivity at high speed and over a medium range. However, as indicated in Table 2.1, several other standards have been developed in the PAN and WBAN applications, which have low data volume, short range, and low power characteristics.

Table 2.1: Typical short-range wireless standards comparison table

Wireless Standards	**Wi-Fi[19]**	**Bluetooth[20]**	**BLE[20]**	**ZigBee[21]**	**Z-Wave [22]**	**ANT+[23]**
Bandwidth	Up to 54Mbps	1-3Mbps	1Mbps	256Kbps	40Kbps	1Mbps
Range	>100m	<100m	<30m	<100m	<30m	<30m
Topology	P2P, Star Tree, Mesh	P2P Star	P2P Star	P2P, Star Tree, Mesh	Mesh	P2P, Tree, Mesh
Security	High	High	High	Medium	High	High
Current Consumption	High	Medium	Ultra-Low	Low	Low	Ultra-Low
Frequency hopping	No	Yes	Yes	No	No	No
Cost	High	Medium	Very low	Low	Low	Very low

Note. The most popular type or version of each standard is listed in this table.

2.1. Wi-Fi

Wireless Fidelity (Wi-Fi) is a generic term that refers to the IEEE 802.11 communications standard, and was originally introduced in 1997 [19]. During the last decade, it has become one of the common standards in wireless-enabled devices such as computers, smartphones, peripheral devices, and network components [18]. The plug-and-play capability, high speed, and medium propagation range along with supporting several network topologies (e.g. star, tree, and peer-to-peer) make Wi-Fi a unique solution for wireless local area networks. A summary of the typical Wi-Fi standard is illustrated in Table 2.2. However, the new IEEE 802.11 standard versions have been improved in some aspects such as maximum signal rate and security.

Table 2.2: Wi-Fi standard specification (Taken from [19])

Specification	state
Frequency band	2.4GHz and 5GHz
Coexistence mechanism	Transmit power control
Multiplexing	DSSS, CCK, OFDM
Future multiplexing	MIMO
Noise adaptation	Physical layer
Typical output power	30-100mW (15-20dBm)
Nominal range	100m
Maximum one-way data rate	31.3Mbps
Basic cell	BSS
Extension of the basic cell	ESS
Topologies	peer-to-peer, star, tree, mesh
Maximum number of devices in the basic cell	Unlimited in ad hoc network (IBSS); up to 2007 devices in the infrastructure networks.
Maximum signal rate	54Mbps
Channel access method	Distributed: CSMA/CA
Channel efficiency	Decreasing with offered traffic
Data protection	32-bit CRC
Procedures used for the network setup	Ad hoc networks: scan, authentication Infrastructure: scan, authentication, association

Authentication	Shared secret, challenge-response
Power save mode	Doze

2.1.1. *Wi-Fi Protocol Stack*

Although the upper layer in the IEEE 802.11 protocol stack is model-dependent, the main layers, including physical (PHY), medium access control (MAC) and logical link control (LLC) layers are permanent in the Wi-Fi firmware. Figure 2.1 demonstrates the IEEE 802.11 protocol stack versus OSI and TCP/IP models [19]-[24].

Figure 2.1: IEEE 802.11 protocol stack vs. OSI and TCP/IP models (Taken from [19])

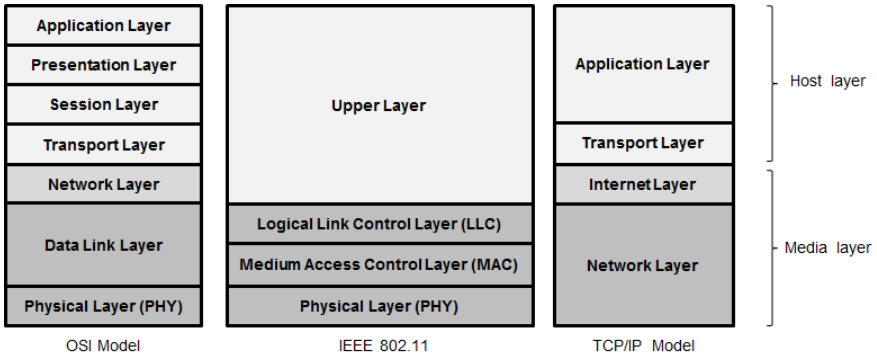

2.1.2. *Wi-Fi MAC Frame Format*

The IEEE 802.11 general MAC frame (see Figure 2.2) consists of a MAC header, the frame body (i.e., payload), and a frame check sequence (i.e., CRC32) [19].

Figure 2.2: IEEE 802.11 MAC frame format (Taken from [19])

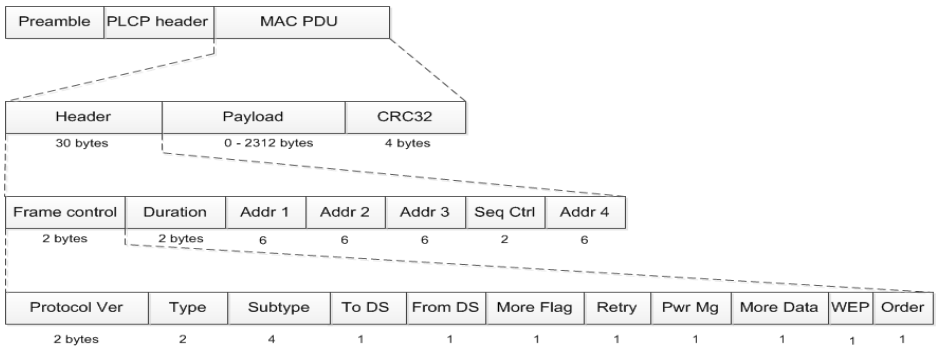

2.1.3. *Wi-Fi Network Topologies*

The Wi-Fi standard supports the independent basic service set (IBSS) and extended service set (ESS) in the form of logical architecture as well as peer-to-peer, star, tree, and mesh, known as physical network topologies. The main components of logical architecture consist of a station (STA), wireless access point (AP), basic service set (BSS), and distribution system (DS). With regard to the network topology, IEEE 802.11 has defined two operating modes, infrastructure and ad hoc (see Figure 2.3), to deploy several physical network topologies.

Figure 2.3: Wi-Fi network topologies (Taken from [19])

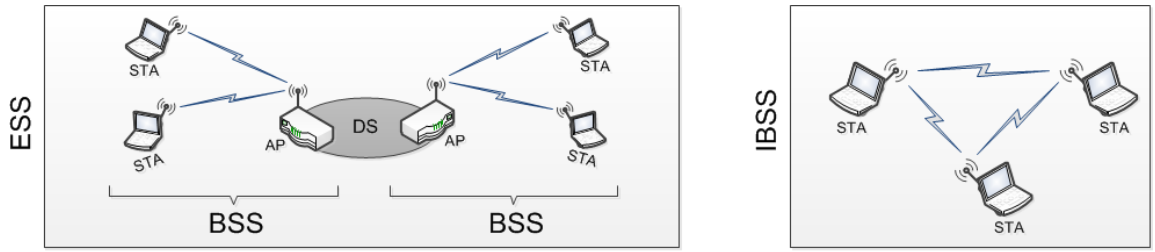

2.2. Bluetooth

Bluetooth is an open proprietary wireless technology based on the IEEE 802.15.1 standard for short-range wireless communication between several devices in the industrial, scientific, and medical (ISM) band at 2400 MHz to 2485 MHz radio frequencies [20]. It was originally created by Ericson[4] in 1994 in order to provide a wireless alternative to the RS232 serial communication. Bluetooth technology utilizes the adaptive frequency hopping (AFH) technique to take advantage of available frequency in the shared 2.4GHz spectrum and to diminish the interference of other wireless technologies in this band. The AFH technique not only acts as a robust communication feature for Bluetooth, but also makes possible the coexistence of other wireless

[4] http://www.ericsson.com/

technologies in electronic devices such as laptops and smartphones. Although this standard was introduced by versions 1.0 and 1.0B, the core specification version 1.1 is known as the first successful Bluetooth standard as it corrected earlier versions' bugs and problems. However, Bluetooth core 1.2 was developed in order to enhance the transmitting/receiving speed and to support the hardware controller interface (HCI) for a three-wire universal asynchronous receiver and transmitter (UART). Afterwards, the Bluetooth standard developed core specification versions 2.0, 2.1+EDR, 3.0 and 4.0[5], and adapted its capabilities to become a main part of PANs. The Bluetooth propagation range is mandated by power class radios 1, 2, and 3 for 1, 10, and 100 meters respectively. Table 2.3 demonstrates the specification of Bluetooth core version 2.1+EDR.

Table 2.3: Typical Bluetooth standard (Taken from [20])

Core version	2.1 + EDR
Frequency band	2.4-2.485GHz ISM band
Coexistence mechanism	Adaptive frequency hopping
Multiplexing	FHSS
Future multiplexing	UWB
Noise adaptation	Link layer
Typical output power	Class 1=100mW (20dBm), Class 2=2.5mW (4dBm), Class 3=1mW (0dBm)
Operating range	Class 1=100m, Class 2=10m, Class 3=1m
Maximum one-way data rate	2.1Mbps
Basic cell	Piconet
Extension of the basic cell	Scatternet
Topologies	Peer-to-peer, star
Maximum number of devices in the basic cell	8 active devices and 255 in park mode
Maximum signal rate	3Mbps

[5] The newest version of the Bluetooth family, core 4.0, is known as Bluetooth low energy and it is scholarly discussed in this thesis.

Channel access method	Centralized: TDMA
Channel efficiency	Constant
Data protection	16-bit CRC (ACL links only)
Procedures used for the network setup	Inquiry, Page
Authentication	Shared secret, Pairing
Power save mode	Sniff, Hold, Park, Standby

2.2.1. *Bluetooth Protocol Stack*

The IEEE 802.15.1 standard structures the Bluetooth protocol stack in the form of four main layers: radio, baseband, link manager, and L2CAP [25]. In addition to these layers, there are several modules, services, profiles and applications that manage Bluetooth functionalities and operations (see Figure 2.4).

Figure 2.4: Bluetooth protocol stack (Taken from [25])

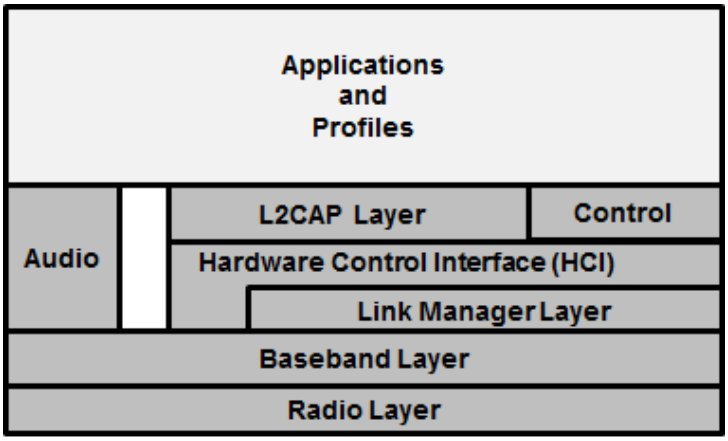

2.2.2. *Bluetooth Packet Format*

The Bluetooth packet format consists of access code, header, and payload (see Figure 2.5), with access code being 68 or 72, header 54, and payload 0 to 2745 bytes [25]. There are three Bluetooth packet types as follows:

- Access code only (shortest packet format)
- Access code and header
- Access code, header and payload

Every packet starts with the access code, whether the access code length is 68 bytes or 72 bytes. If its length is 72 bytes, the header comes next and the packet may or may not include payload.

Figure 2.5: Bluetooth general packet format (Taken from [25])

2.2.3. *Bluetooth Network Topologies*

Considering the IEEE 802.15.1 standards, there are point-to-point and point-to-multipoint network architectures that provide piconet topology for Bluetooth in the simplest form and scatternet topology in the extended structure (see Figure 2.6) [25]. Each piconet comprises only one master node and at least one slave node. A scatternet is two or more piconets that have common nodes. However, the common node can be a master node in one piconet and slave node in another piconet, or play the role of a slave role in both piconets.

Figure 2.6: Bluetooth network topologies (Taken from [25])

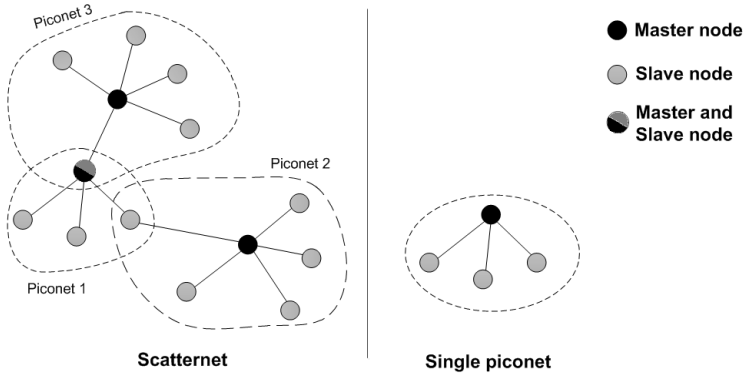

2.3. Bluetooth Low Energy

Bluetooth low energy[6] is a feature of Bluetooth core specification version 4.0, aiming for ultra-low peak, average, and idle mode power consumption as well as low cost. Bluetooth SIG introduced BLE in 2009 to facilitate a wide range of applications in home automation, healthcare, security, home entertainment, fitness, and sports. Table 2.4 presents typical specifications of the Bluetooth low energy protocol [20].

Table 2.4: Bluetooth low energy (Taken from [20])

Core version	4.0
Frequency band	2.4-2.485GHz ISM band
Coexistence mechanism	Adaptive frequency hopping
Modulation	GFSK
Noise adaptation	Link layer
Typical output power	Min= 0.01mW (-20dBm) , Max= 10mW (+10dBm)
Operating range	Max=100m (+10dBm)
Maximum one throughput	256Kbps
Basic cell	Star (Master-Slaves)
Extension of the basic cell	Star-Bus
Topologies	Peer-to-peer, star
Maximum number of devices in the basic cell	Unlimited
Maximum signal rate	1Mbps
Channel access method	TDMA, FDMA
Data protection	AES-128
Authentication	Secure simple pairing
Power save mode	Standby

[6] Although BLE is produced in single and dual modes, the purpose of BLE in this thesis is single-mode Bluetooth low energy and thus it is simply referred to as BLE.

2.3.1. *BLE Protocol Stack*

The BLE protocol stack employs the low energy profile in order to consume as low energy as possible during the operation. Figure 2.7 illustrates that the BLE protocol stack, unlike the Bluetooth standard, does not have any audio capability. The BLE protocol stack layers are described as follows [26]:

- **The Physical Layer (PHY)**: transmits and receives GFSK packets over the physical channel at 1Mbps on the 2.4GHz ISM band.
- **The Link Layer (LL**): controls the RF states of the transceiver consisting of advertising, scanning, initiating, connected, or standing by states.
- **The Host-Controller Interface (HCI)**: processes all communications between the host and controller, usually by SPI, USB, or a UART.
- **The L2CAP**: provides data encapsulation services, traffic management, controls the order of submission of protocol data unit to the baseband and ensures QoS access to the physical channel.
- **The Attribute Protocol (ATT)**: allows a device to expose a specific data format known as attributes to another device. The device exposing attributes is introduced as server and the other is referred to as client.
- **The Security Manager (SM)**: generates, manages, and stores encryption and identity keys to enable two devices to communicate securely over a dedicated L2CAP channel. Bluetooth Low Energy uses 128-bit AES encryption with counter mode CBC-MAC and a user-defined application layer.
- **The Generic Attribute Profile (GATT)**: defines the sub-procedures for using ATT and specifies the structure of Bluetooth profiles.
- **The Generic Access Profile (GAP)**: block provides the interface between the application and Bluetooth profiles and handles device discovery, connection, and services, including security procedures.

Figure 2.7: Bluetooth low energy protocol stack (Taken from [27])

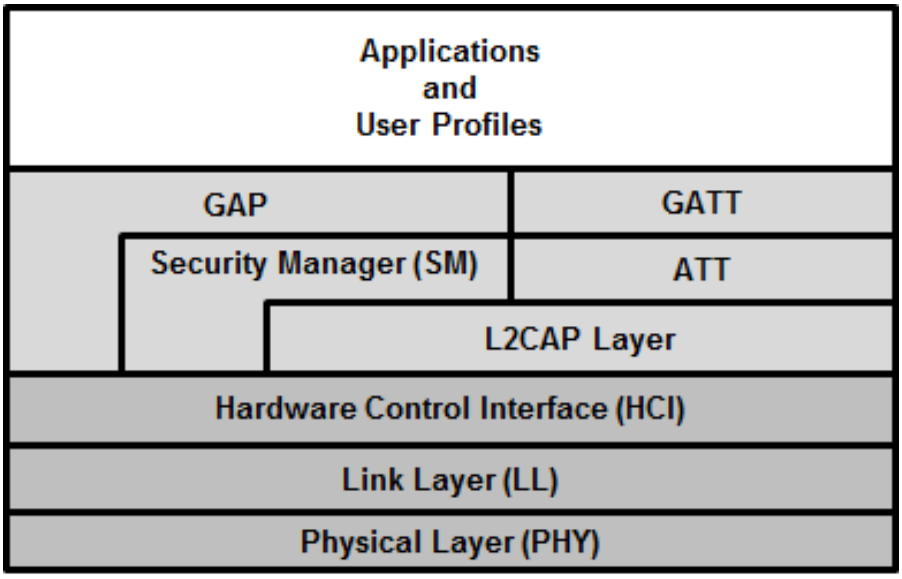

2.3.2. *BLE Packet Format*

The BLE link layer has only one packet format for both advertising and data packet channels. Figure 2.8 illustrates this packet format, which constitutes preamble, access address, PDU, and CRC fields, with preamble, access address and CRC having a constant length of 1, 4, and 3 octets respectively. In contrast, PUD is variable between 2 and 39 octets [27].

Figure 2.8: Bluetooth low energy packet format (Taken from [27])

2.3.3. *BLE Operation States*

Bluetooth low energy operates under five state machines, consisting of standby, advertising, scanning, initiating, and connection (see Figure 2.9). These states facilitate four roles in the GAP layer for a BLE device as follows [27]:

- **Broadcaster**: an advertiser that is non-connectable.
- **Observer**: scans for advertisements, but cannot initiate connections.

- **Peripheral**: an advertiser that is connectable. This device is called slave after connection.
- **Central**: scans for advertisements and initiates connections. This device is called master after connection.

Although each BLE device is able to have a certain combination of multiple roles, it is only allowed to play one of these roles at each time instant.

Figure 2.9: State machine diagram of the BLE operation states (Taken from [27])

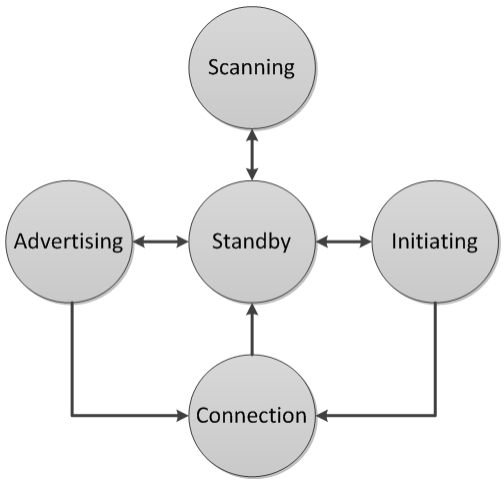

2.3.4. *BLE Network Topologies*

The BLE protocol supports peer-to-peer and star network topologies containing only one master and one or more slave devices (see Figure 2.10). The master node initiates connection, and each branch device that accepts the connection is a slave node. The Bluetooth low energy technology uses a 32-bit access address on every packet for each slave and theoretically allows billions of devices to be connected. However, in practice, there are some issues such as memory and inter-piconet interference that limit the maximum number of nodes in a piconet [28].

Figure 2.10: BLE network topology (Taken from [27])

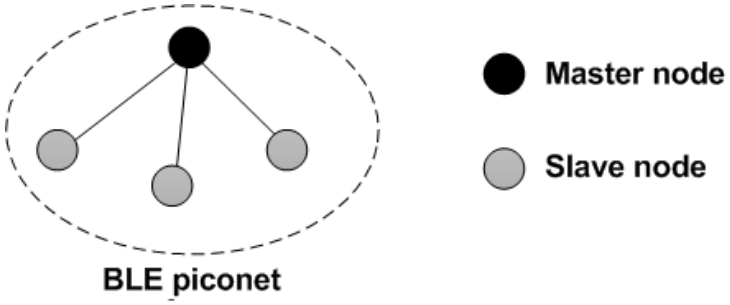

2.4. ZigBee

The ZigBee specification is a wireless standard for WPAN according to IEEE 802.15.4 that operates in both 2.4GHz ISM and sub-gigahertz 868/915MHz frequency bands [21]. The first approach to creating ZigBee took place in 1998; however, the ZigBee alliance began building the ZigBee specification on top of the IEEE 802.15.4 standard in 2003 and announced the first version of ZigBee in 2004. In contrast to Bluetooth and BLE, ZigBee is able to support mesh network topology. Table illustrates the specification of a typical ZigBee standard version 2007.

Table 2.5: Typical ZigBee specification (Taken from [21])

version	2007
Frequency band	2.4GHz ISM band and 868/915MHz sub-gigahertz
Modulation	OQPSK and BPSK for 2.4GHz and 868/915MHz respectively
Typical output power	Min= 1mW (0dBm), Max= 100mW (+20dBm)
Operating range	Max=+100m (+20dBm)
Throughput	256Kbps (2.4GHz), 40Kbps (915MHz), 20Kbps (868MHz)
Topologies	Peer-to-peer, star, tree, mesh
Maximum number of devices in the network	65000+
Channel access method	CSMA-CA
Data protection	AES-128
Authentication	CBC-MAC
Power save mode	Standby

2.4.1. *ZigBee Protocol Stack*

The ZigBee protocol stack is designed based on the IEEE 802.15.4 standard and is built on a PHY and MAC layer foundation (see Figure 2.11). This protocol stack consists of the network (NWK) layer and framework for the application layer. The application layer framework comprises an application support sub-layer (APS) and ZigBee device object (ZDO) [21].

Figure 2.11: ZigBee protocol stack (Taken from [21])

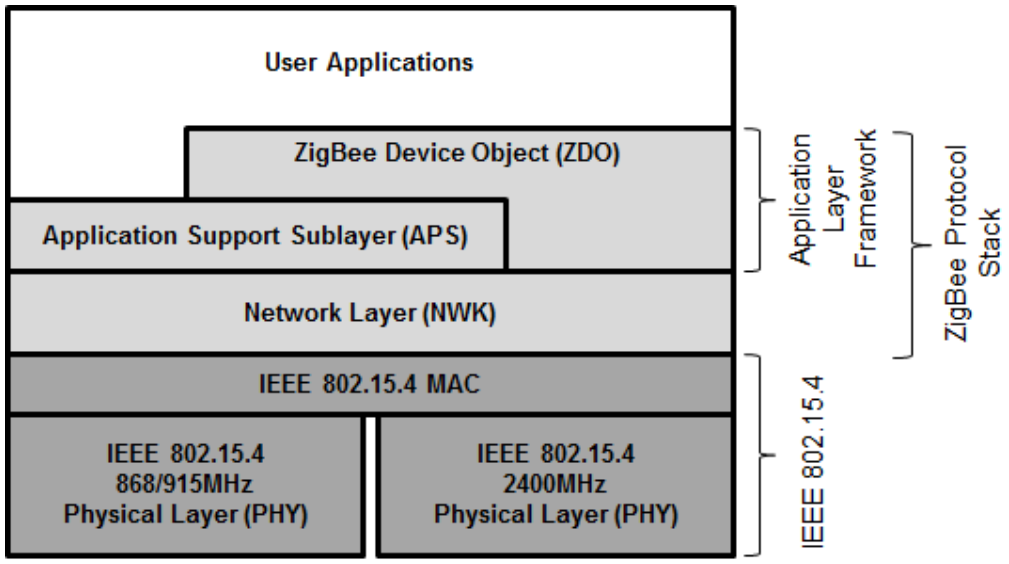

2.4.2. *ZigBee Frame Format*

The ZigBee frame format is defined based on the IEEE 802.15.4 PHY layer and MAC sub-layer data frame [21]. Figure 2.12 illustrates ZigBee frames containing NWK and APS in which NWK frames are formed in the MAC sub-layer payload. The NWK frame has two parts, NWK payload, and NWK header (HDR). The NWK payload is utilized for the APS frame and HDR provides network-level addressing and control information. However, the APS frame is formed by applications and facilitates tasks such as application-level addressing, control information, and the security mechanism [29].

Figure 2.12: ZigBee frame format (Taken from [21])

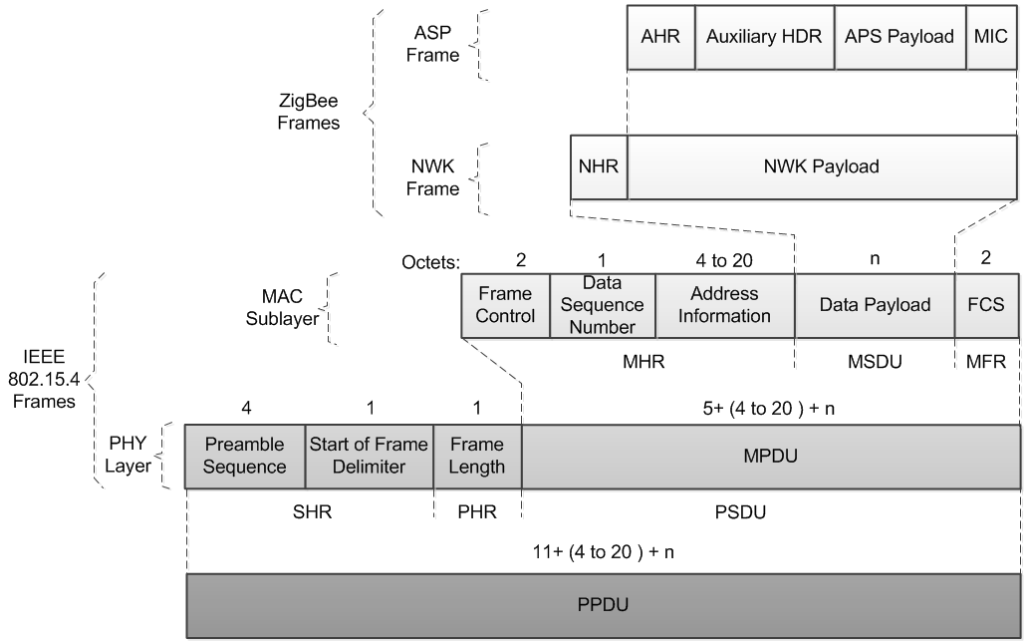

2.4.3. *ZigBee network topology*

The IEEE 802.15.4 supports star and peer-to-peer network topologies and performs the required structures for the ZigBee NWK layer to be designed for providing star, tree and mesh network topologies [21]. The ZigBee standard is composed of several device types including ZigBee coordinator, router, and end device. Regarding network topology, all or some of these devices exist in the network. In the star topology, a single ZigBee coordinator node manages the network and all other nodes the end devices. However, the mesh and tree topologies, in addition to these two devices, utilize the ZigBee router in order to extend the network (see Figure 2.13). Indeed, a cluster tree network consists of a number of connected star networks whose central nodes are also in direct communication with the single ZigBee coordinator. Considering a set of routers and a single coordinator, the network is formed into an interconnected mesh of routers and end nodes that pass information from node to node using the most cost-effective path. If any individual router becomes inaccessible, an alternate router can be discovered automatically and transfer network traffic.

Figure 2.13: ZigBee network topologies (Taken from [21])

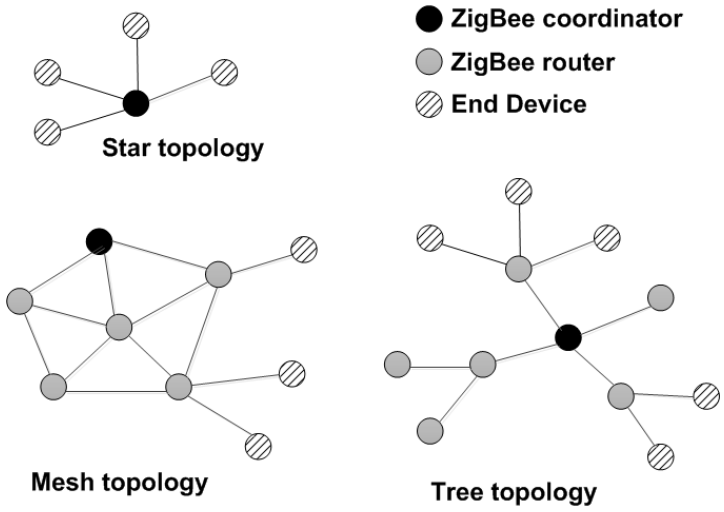

2.5. Z-wave

Z-Wave is a proprietary short-range wireless communication protocol that operates in the sub-gigahertz radio frequency band around 900MHz. It supports mesh network topology with a maximum of 232 nodes [22]. Z-Wave technology is created to provide wireless-enabled consumer electronic products for home automation. The Z-Wave protocol stack consists of RF media, MAC, transfer, routing and application layers. Figure 2.14 demonstrates the Z-Wave MAC frame format.

Figure 2.14: Z-Wave MAC frame format (Taken from [22])

2.6. ANT+

ANT is a proprietary wireless communication technology working in the 2.4GHz ISM radio frequency spectrum created by Dynastream Innovations Inc.[7] for PANs. ANT+ is an inter-protocol added to ANT technology in order to facilitate data collection and routing in the managed network [23]. It is able to support peer-to-peer, star, tree and mesh network topologies with over 65000 nodes. Moreover, it benefits from ultra-low power consumption technology that is ideal for wireless sensor networks. The ANT+ protocol stack consists of radio, protocol, and user defined layers. Figure 2.15 illustrates a comparison between ANT+ protocol and OSI models.

Figure 2.15: ANT+ technology model vs. OSI model (Taken from [23])

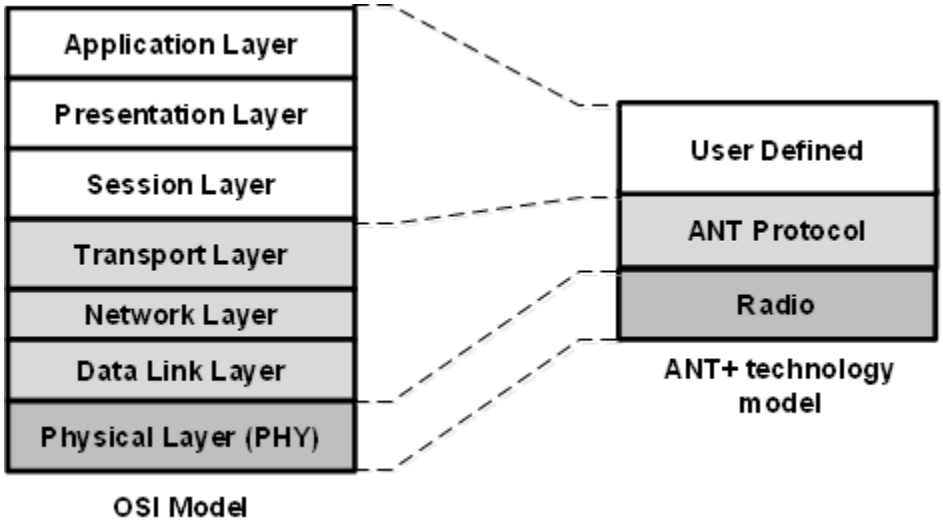

[7] http://www.dynastream.com/

Chapter 3: PV Module Performance Monitoring System Using ZigBee Technology

Various studies have shown that a significant reduction in output power and degradation of the performance of maximum power point trackers (MPPT) are possible under non-ideal conditions [30]. Finding the faulty or malfunctioning PV modules can significantly increase the system down-time of a solar PV power plant and consequently its LCOE rises. Hence, monitoring and detection of non-ideal conditions is a critical issue in PV modules. Several studies have been conducted in the area of PV module performance monitoring system. For example, using a reference solar cell in PV module performance monitoring was studied in [31], but it has a main drawback due to the cost of the required additional PV module.

In this chapter, the concept of a solar photovoltaic (PV) performance monitoring system is introduced by utilizing a ZigBee wireless embedded system that is inside the junction box of the module. The proposed system is able to monitor the performance of PV panels to detect non-ideal operating conditions. ZigBee wireless technology has been selected in this application because of its features in terms of low cost, capability to be used in a mesh network topology, low power consumption, and small form factor (see Table 2.1). The mesh network topology can not only covers a wide area of PV modules distributed in a solar PV power plant but also facilitates deployment of a redundant data communication network between PV modules and a central monitoring system. Moreover, ZigBee technology operates in low power conditions that make it possible to build low power consumption wireless devices. This is essential for a high performance PV module performance monitoring system because the PV module has to supply the power drive of the added circuit. On the other hand, the ZigBee module can be built with a low cost ZigBee-enabled microcontroller and a few extra components that provide a small form factor and low cost device to be installed in the PV module junction box. In summary, the work performed consists of the design and development of a low-cost small form factor electronic hardware embedded module using a ZigBee-enabled

microcontroller. The embedded system software comprises a back-end embedded program and front-end graphical user interface (GUI) that are developed to perform remote monitoring of voltage, current, and power for an array of PV modules. The results of implementation on a proof-of-concept test-bed consisting of two embedded controllers installed on two PV modules are presented in this chapter. The experimental results indicate that the proposed system can provide a low-cost and reliable performance monitoring system for possible utilization in PV power plants.

3.1. System design

The design procedure consists of separating the desired system into two main components: hardware and software with each component divided into several other modules. In the following, we discuss these separately to gain a comprehensive understanding of the entire system. Figure3.1 illustrates the embedded hardware blocks to be utilized for monitoring the PV unit using a ZigBee wireless network utilizing a star topology comprised of a remote device and central station. The remote device addresses a PV module that is equipped with an end device (ED) and sensing devices. The end device provides ZigBee wireless connectivity as well as local process for the PV module's current and voltage sensing, respectively. A step-down DC-to-DC voltage converter that converts the DC voltage of the PV module to a 3.3V DC voltage provides the power to drive the embedded device inside the PV module. On the other side, the coordinator and host PC constitute the central station. Both the ED and coordinator employ a ZigBee-enabled system-on-chip (SoC) in order to perform over-the-air communication between the remote device and a central station. The coordinator facilitates data flow between the ED and host PC in the central station. The host PC is equipped with a graphical user interface (GUI) developed by NI LabView environment[8] in order to carry out real-time performance monitoring of PV modules. The system design consists of the several components described below:

[8] NI LabView: http://www.ni.com/labview

Figure 3.1: PV module performance monitoring system block diagram

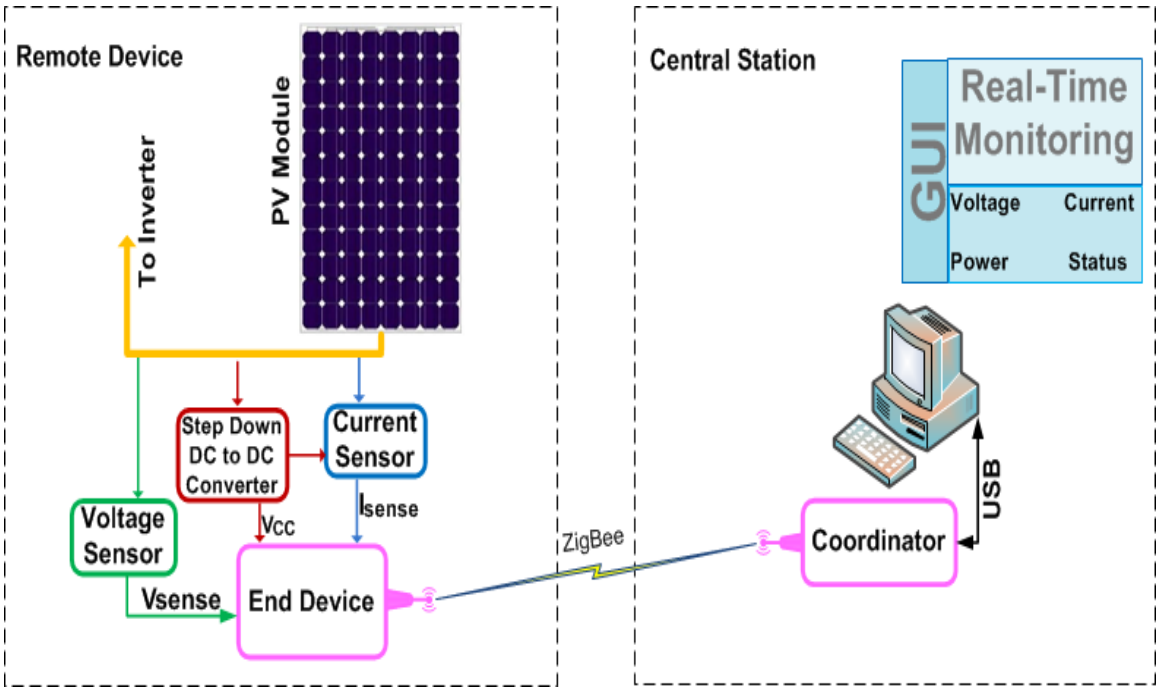

3.1.1. *Hardware components*

The hardware components of the embedded computing system include an end device, voltage sensing, current sensing, a step-down DC-to-DC voltage converter, and the coordinator, as described in detail in the following:

3.1.1.1. Remote Device

Figure 3.2 illustrates the block diagram of the remote device and the connection between its components. The resistive voltage divider and high-side current-sense amplifier measure the voltage and current of the PV module, respectively, and deliver those values to the analog-to-digital converter (ADC) port of SoC. The step-down DC-to-DC voltage converter acts as the power driver for the end device and current sensing circuit.

Figure 3.2: Remote device block diagram

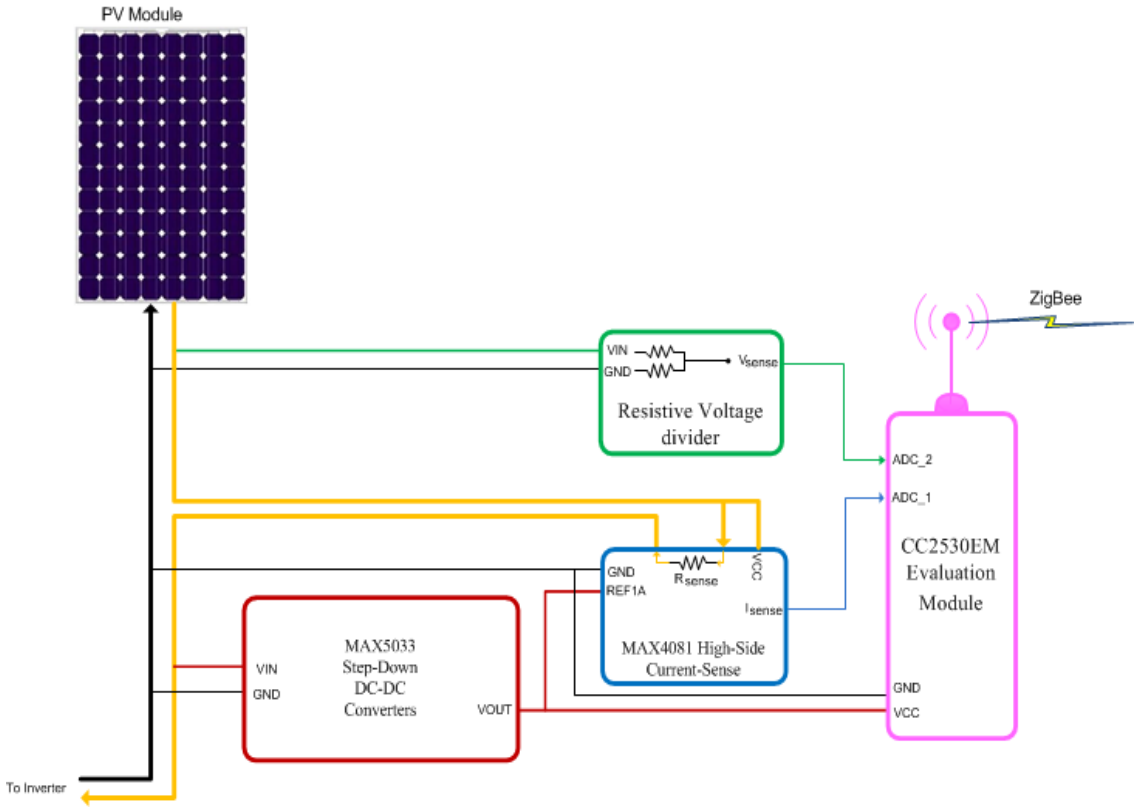

3.1.1.2. End Device

The end device is responsible for transmitting PV module characteristics to the coordinator through ZigBee radio. The core of the end device is TI CC2530, which is an ultra-low power consumption SoC with an optimized 8051 MCU core and ZigBee/IEEE 802.15.4 compliant radio for the 2.4 GHz unlicensed ISM band [32]. This device enables industrial grade applications by offering state-of-the-art noise immunity, excellent link budget, and low voltage operation. In addition, the CC2530 provides extensive hardware support for packet handling, data buffering, burst transmissions, data encryption, data authentication, clear channel assessment, link quality indication, and packet timing information. Owing to ultra-high integration, few external components are required for the operation of this chip (see Figure 3.3).

Figure 3.3: TI CC2530 SoC typical circuit

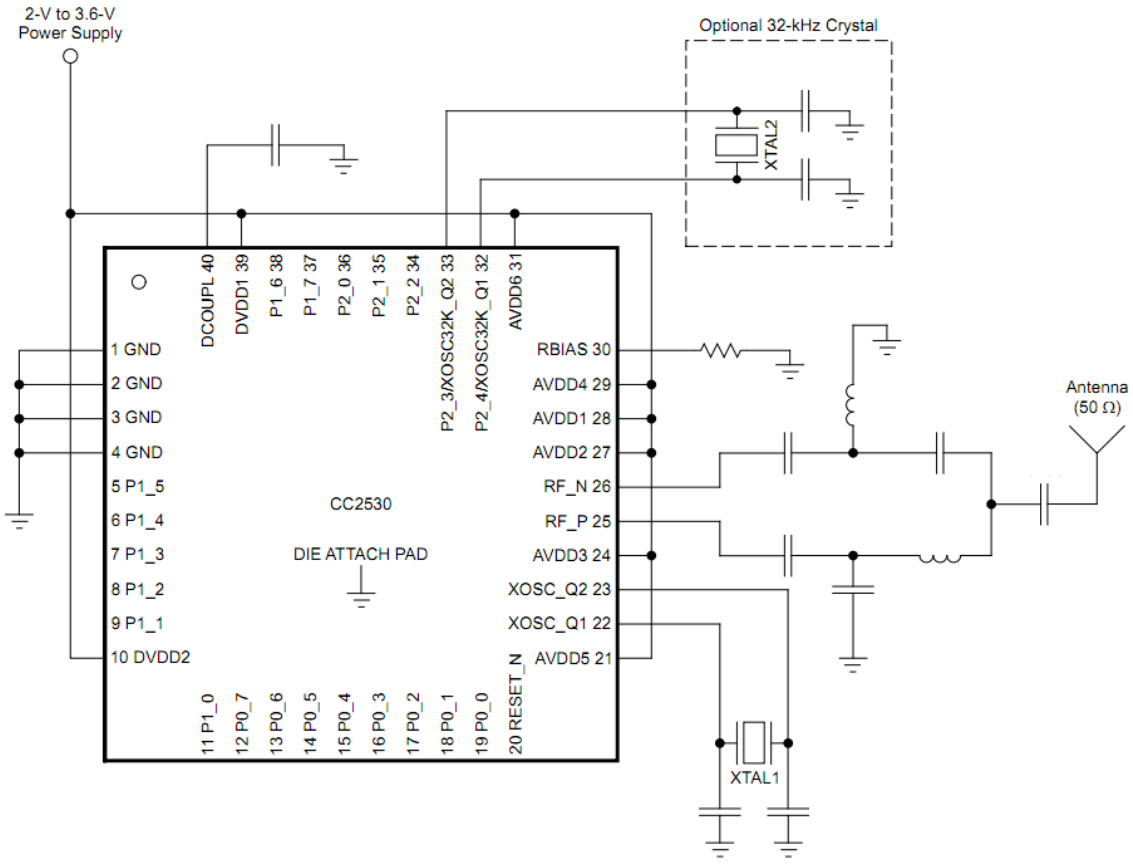

The CC2530 has 21 general-purpose I/O pins (19× 4 mA, 2× 20 mA) and 8 channels of these I/O pins can be programmed to perform 14-bit analog-to-digital conversion with up to 12 bits effective number of bits (ENOB). Moreover, the reference voltage of these ADCs are selectable as internal, external single-ended, external-differential, or AVDD5 [32]. Having an accurate step-down DC-to-DC converter makes AVDD5 a suitable reference voltage for this design (see Appendix A). These features were utilized to convert analog output voltage of the current and voltage sensing circuits.

In this project, a CC2530EM evaluation module (see Figure 3.4a) was used to avoid wasting time on CC2530 circuit fabrication. This module contains the RF IC and necessary external components and matching filters for getting the most out of the radio [33]. The module can be plugged into the SmartRF05EB for purposes of CC2530 programming and debugging. The SmartRF05EB (see Figure 3.4.b) is a platform for

evaluation modules (EM) and can be connected to the PC via USB to control the evaluation modules [34]. In addition, the System-on-Chip Battery Board (SoC-BB) [35] is utilized in order to facilitate connection between CC2530EM and other hardware in the remote device.

Figure 3.4: The CC2530EM evaluation module (a) and SmartRF05EB evaluation board (b)

3.1.1.3. Current Sensing Circuit

The MAX4081 was employed to measure the PV module current, which is essentially a bidirectional high-side current-sense amplifier [36]. It features a 4.5VDC to 76VDC input common-mode range in three gain versions, 5V/V, 20V/V, and 60V/V (see Appendix B). This feature allows the monitoring of current output of a PV module with voltage fluctuations as low as 4.5V. Furthermore, it features high-side current sensing at voltages greater than the supply voltage (VCC). The MAX4081 monitors current through a current-sense resistor and amplifies the voltage across the resistor. The 76V input voltage range of the MAX4081 applies independently to both supply voltage (VCC) and common-mode, input-sense voltage (VRS+). The MAX4081 charging current is represented by an output voltage from VREF to VCC, while the discharge current is given from VREF to GND. Measurements of OUT with respect to VREF yield a positive and negative voltage during charge and discharge. Figure 3.5 illustrates how the current sensing circuit is connected to other modules in the remote device.

Figure 3.5: Current sensing circuit for the PV module

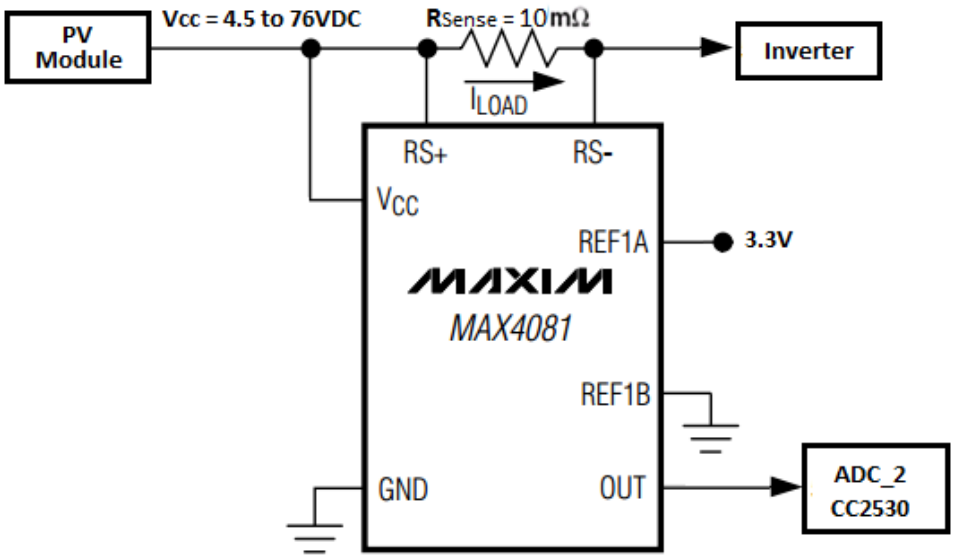

Ideally, the maximum load current results in a full-scale sense voltage across the current-sense resistor given by,

$$V_{OUT} = V_{SENSE} \times A_V \qquad (3.1)$$

where V_{SENSE} is the full-scale sense voltage ($\pm 500mV$, $\pm 250mV$ and $\pm 125mV$ for gains 5V/V, 20V/V, and 60V/V, respectively) and A_V is the voltage gain of the device. Considering a 20V/V gain and 10mΩ current sense resistor in this design, the maximum V_{OUT} is 2.5V.

3.1.1.4. Voltage Sensing Circuit

Considering the DC signal of a PV module and high input impedance of the analog to digital converter (ADC_2) in the CC2530, a simple voltage divider circuit consisting of two resistors in series is appropriate for a voltage sensing circuit. The resistors should be arranged to have the maximum V_{SENSE} voltage equal to 3.3VDC for application to the CC2530 analog to digital converter channels. Hence, the voltage divider formula for the voltage sensing circuit is given by

$$V_{sence} = V_{IN} \times \frac{R_2}{R_1 + R_2} \qquad (3.2)$$

where V_{sence} is the sensing voltage, V_{IN} is PV module voltage, R_1 and R_2 are series resistors, respectively. Figure 3.6 illustrates the voltage sensing circuit in which a PV module with a 28VDC open circuit voltage is utilized. Considering a value of 3.3VDC for maximum V_{sence} and solving (3.2 for the series resistors, the values R_1 and R_2 are obtained as 47kΩ and 6.3kΩ, respectively.

Figure 3.6: Voltage Sensing Circuit

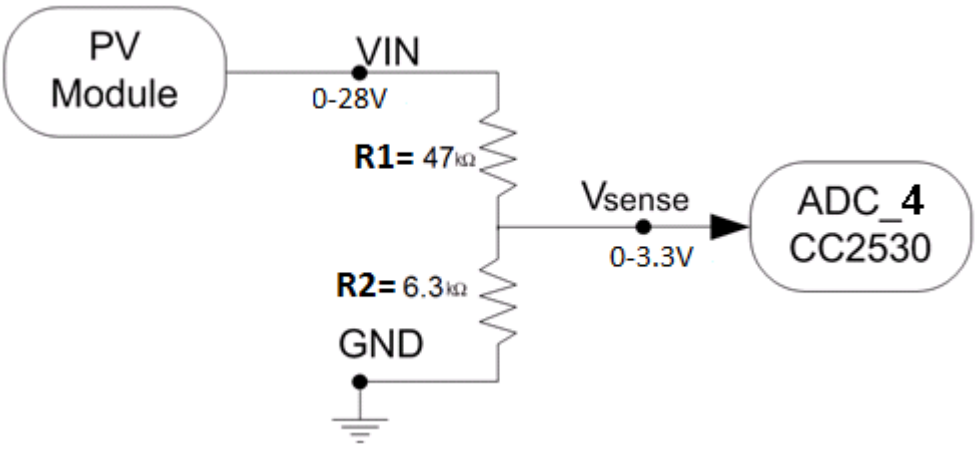

3.1.1.5. Step-Down DC-to-DC Converter

A step-down DC-to-DC converter is needed to provide the DC power drive for the end device and current sensing circuit. Figure 3.7 illustrates a step-down DC-to-DC converter based on the MAX5033D chipset [37]. The MAX5033D is a high-efficiency, high-voltage, step-down DC-to-DC converter that operates from an input voltage up to 76V and consumes only 270µA quiescent current at no load. This pulse-width modulated (PWM) converter operates at a fixed 125 kHz switching frequency at heavy loads, and automatically switches to pulse-skipping mode to provide low quiescent current and high efficiency at light loads. The MAX5033D includes internal frequency compensation simplifying circuit implementation. The device uses an internal low-on-resistance, high-voltage, DMOS transistor to obtain high efficiency and reduce overall system cost. This device includes under voltage lockout, cycle-by-cycle current limit, hiccup-mode output short-circuit protection, and thermal shutdown. The MAX5033D delivers up to 500mA output current and provides an adjustable output voltage, from 1.25V to 13.2V (see Appendix C).

Both the end device and current sensing circuit operate with 3.3V DC, and consequently the component values in Figure 3.7 are calculated to meet this need. Moreover, the total current consumption of these circuits is less than 100mA, which is below the MAX5033D maximum rating.

Figure 3.7: Step-down DC-to-DC converter schematic

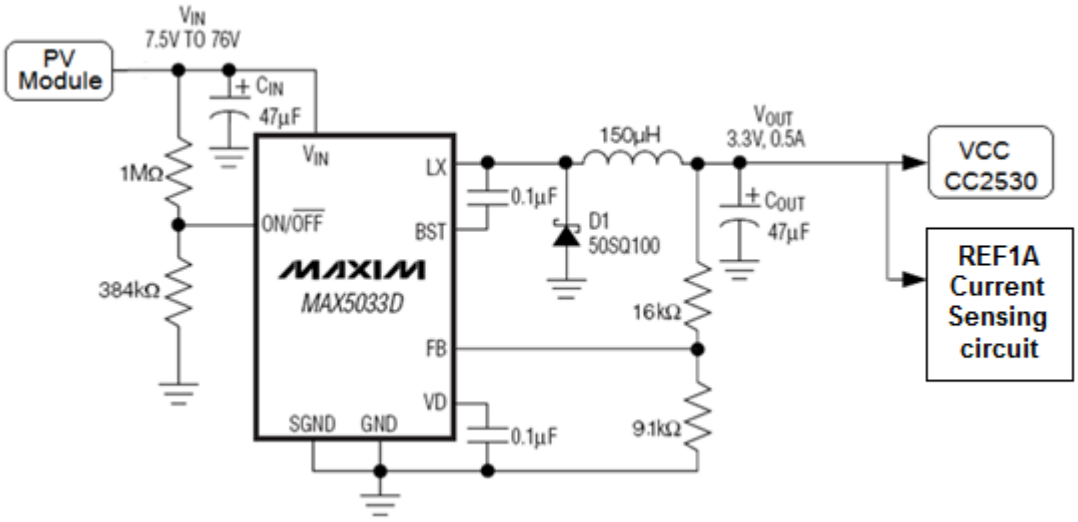

3.1.1.6. Central Station

The central station contains a coordinator that is a fully operational ZigBee-enabled USB dongle device, and a host PC equipped with graphical user interface (GUI) (see Figure 3.1). The USB dongle employs a TI CC2531 SoC and facilitates data communication between the PV panels and GUI through ZigBee connectivity (see Figure 3.8). The CC2531 is identical to the CC2530, with the addition of a built-in full speed USB 2.0 compliant interface [32].

Considering gradual variations of voltage and current in the PV panel, the RS232 protocol is utilized for data communication between the USB dongle and host PC. Although taking advantage of the RS232 communication tool in the NI LabView (GUI) environment is straightforward, the plug and play features of USB connectivity simplify operation. Hence, the coordinator performs a virtual serial protocol for communication between the CC2531 USB dongle and LabView. For this purpose, the LabWindows/CVI

instrument driver development wizard is employed to create the USB to virtual RS232 serial driver.

Figure 3.8: CC2531 USB dongle

The performance of the PV module can be monitored on the host PC via a graphical user interface that was developed using the NI LabView environment. This GUI not only demonstrates real-time voltage and current signal levels but also provides information on module status. Moreover, the calculated power is displayed in order to investigate the performance of the modules.

3.1.2. *Software design and development*

The embedded software developed in this work consists of back-end embedded programs implemented on the MCU platforms CC2530 and CC2531 from Texas Instruments and the front-end graphical user interface developed on the host PC. The software algorithms and program details are discussed in the following sections. The back-end embedded software was programmed using C-language by taking advantage of the TI ZigBee protocol stack [32] and the IAR Embedded Workbench[9] integrated development environment (IDE). This IDE tool supports compiling and debugging of the CC253x SoC family through the SmartRF05EB. Moreover, it is bundled with all the files required for CC253x to start development, such as register definition header files, linker

[9] IAR IDE: http://www.iar.com

command files, driver, and device description files needed for debugging and programming.

3.1.2.1. End Device Embedded Software

The embedded software developed at the end device is responsible for all local operations, including current and voltage sensor reading through ADC, while handling over-the-air data communication between the remote device and central station. The software flowchart depicted in Figure 3.9 illustrates the operation steps. Referring to this feature, following system start up (i.e., board initialization and radio setup), a non-stop loop undertakes the end device's main operations. The main operations constitute PV module voltage and current reading as well as data transfer to the coordinator.

Figure 3.9: End device software module flowchart

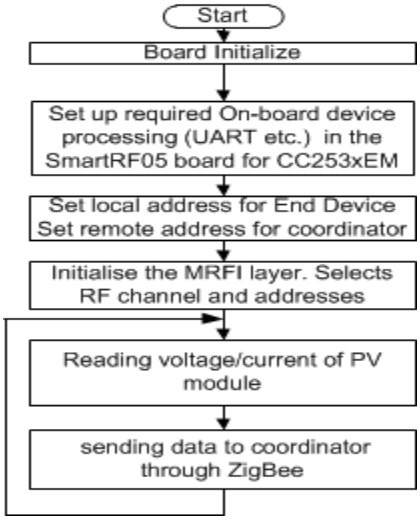

The analog to digital converter API for the TI CC25xx SoC software stack protocol is a 16-bit signed integer (int16) function as follows:

int16 adcSampleSingle (uint8 reference, uint8 resolution, uint8 channel)

It consists of three 8-bit unsigned integer (uint8) input parameters and returns the int16 conversation result for ADC. The supply voltage (i.e., AVDD=3.3V) is employed for ADC voltage reference and the resolution is considered 10bits. However, ADC channels

2 and 4 are selected for PV module current and voltage conversion respectively. The software C code for the end device is in Appendix D.1.

3.1.2.2. Coordinator Embedded Software

The coordinator embedded software performs data handling between the end device and a host PC. Akin to end device embedded software, it begins with board initialization and radio setup and afterwards continues with a non-stop loop that conducts the coordinator's main operations. Figure 3.10 represents the coordinator, which continuously receives data from the end device over-the-air and transmits it to the GUI USB port (i.e., USB to virtual serial port) and the host PC. The software C code for the coordinator is provided in Appendix D.2.

Figure 3.10: Coordinator embedded software module flowchart

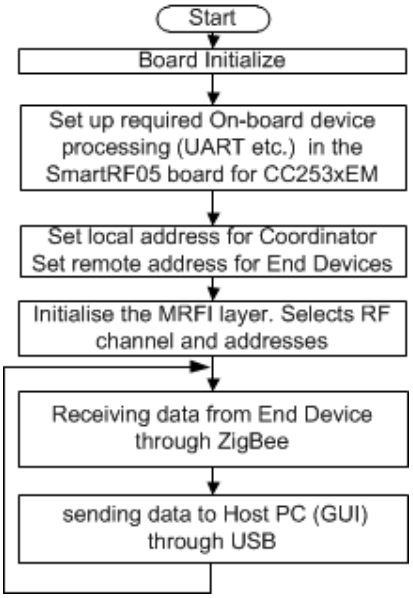

3.1.2.3. Graphical User Interface Software

The graphical user interface performs the monitoring and controlling tasks on the host PC. The GUI was developed using the NI LabView environment, which displays real-time voltage and current values along with the status of each PV module. Figure 3.11 illustrates a view of the graphical user interface flowchart with its LabView code presented in Appendix E.

Figure 3.11: Graphical user interface software flowchart

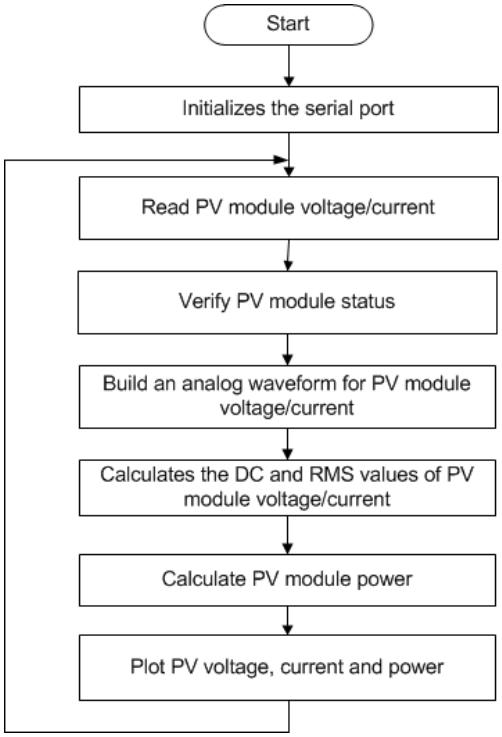

3.2. System Integration

The final stage of the design involves system integration, which is accomplished in accordance with the bottom-up design methodology by means of connecting the individual modules constituting the remote device and central station. Figure 3.12 illustrates components of the remote device that that was utilized in the experiments. On the central PC station, a TI CC2530 USB dongle is used. Furthermore, the software was developed and tested by means of the IAR integrated development environment, which was flashed into both the end device and coordinator using the SmartRF05EB evaluation board.

Figure 3.12: Remote device integrated system

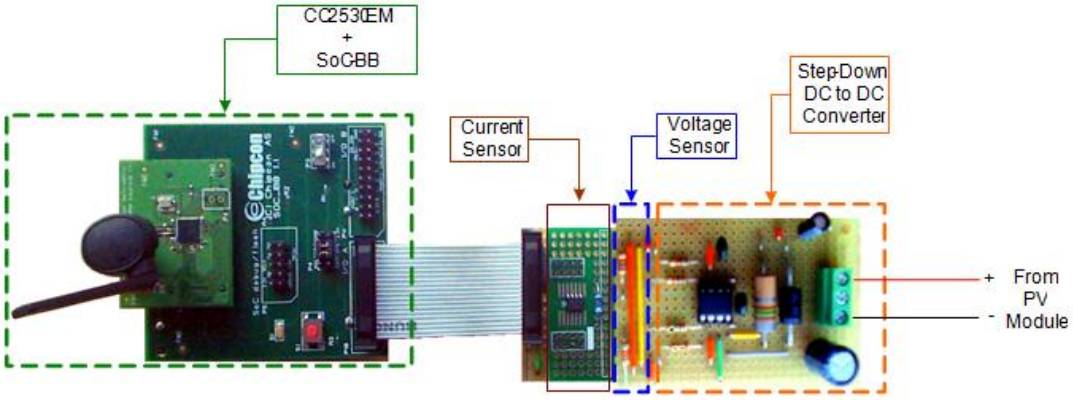

3.3. System Implementation and Experiment

The embedded hardware and software modules are built and integrated in order to evaluate the performance of the PV panels. The prototype system is illustrated in Figure 3.13, consisting of two PV modules equipped with end devices (i.e., ZigBee-enabled end devices), a coordinator (i.e., CC3531 USB dongle), and a monitoring host computer. This setup conducts an experiment on a proof-of-concept test bed for the proposed research.

Figure 3.13: Experimental setup for PV module performance monitoring with two modules

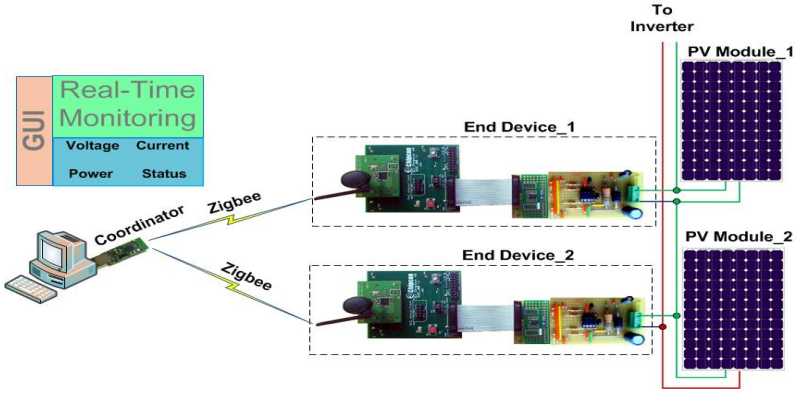

In a practical system, the series connection of PV modules forms “module strings”, which are connected to an inverter. To investigate operation of the monitoring

system, fault conditions due to partial shadowing were introduced by using a curtain in the lab when the module was subjected to sunshine. Considering the PV module's I-V characteristic, when a shadow of about 50% was created on the PV module_1, its current and voltage dropped, as shown in Figure 3.14. In this case, the string and PV module_2 current is the same as that of PV module_1. Consequently, the voltage of the second panel increases due to the I-V characteristic of PV module_2. Figure 3.14 demonstrates the output on the user interface indicating this behavior.

Figure 3.14: Voltage, current and power for two series PV modules under partial shadow represented in GUI

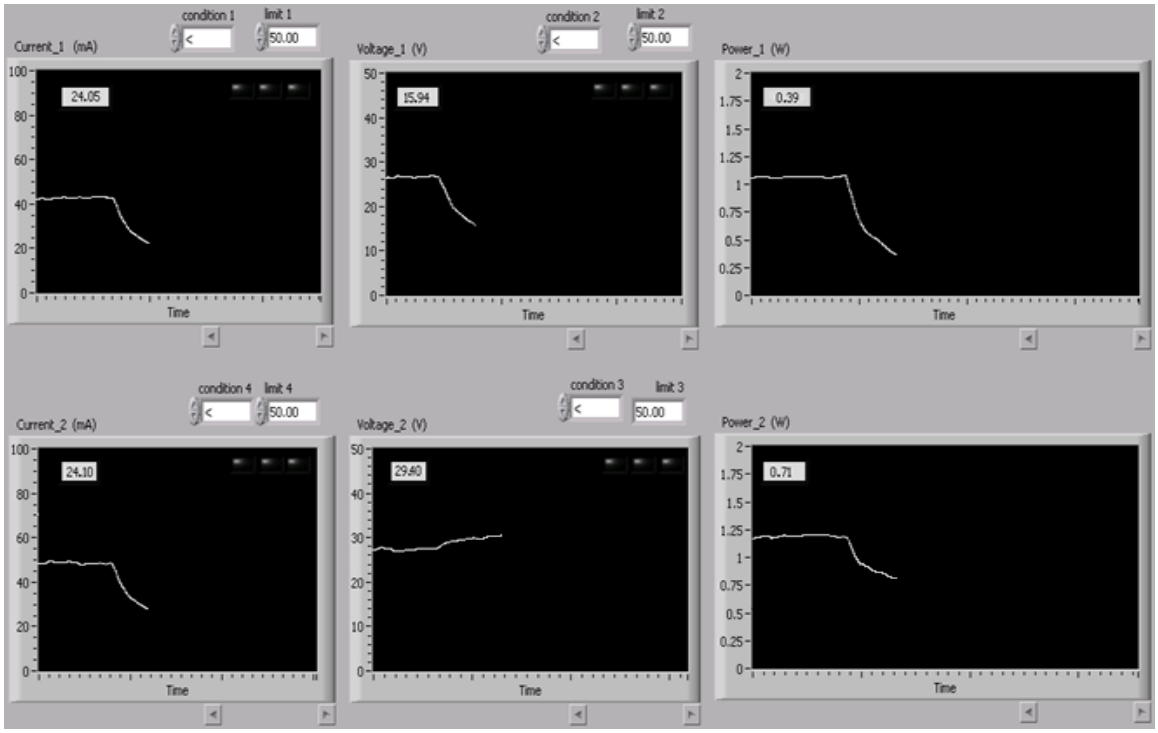

Chapter 4: Energy-efficient Lighting using Bluetooth Low Energy (BLE)

The concept of an energy-efficient lighting system is an attractive research area and it is being studied nowadays. Several research studies have shown that electrical energy use can be significantly lowered by utilizing lighting control systems such as occupancy detectors [38], dimming technologies [39], and daylight harvesting mechanisms [40]. For instance, an occupancy sensor with a 15-20 minute ON-time period in an office can save 20-26% of lighting energy compared to the manual operation of a wall switch [41]. Moreover, by utilizing a combination of daylight harvesting and dimming techniques, additional savings of about 20% can be achieved [41]. The percentages can vary based on the application and environment; for example, in low-occupancy areas, energy savings result mainly from the occupancy sensors, while in areas with high-occupancy, savings are mostly achieved by means of daylight harvesting and dimming [41]. Thus, the appropriate energy-efficient lighting systems rely on these techniques and control mechanisms that manage the relation between occupancy sensors, daylight harvesting, and dimming based on the application environment (e.g., office building, warehouse, or residential environments). However, the controller module needs communication technologies for access to several parts of the energy-efficient lighting system. Several researches have been conducted on wired technologies for energy-efficient lighting systems [42]-[43], but they have some drawbacks in terms of the cost of new cabling and installation for retrofitted buildings. To overcome the wiring problem, wireless technologies have recently been introduced and they are becoming more and more popular in the area of building automation and energy-efficient applications, and so have created new research fields. For instance, ZigBee wireless connectivity was studied in several applications for intelligent and energy-efficient lighting systems [44]-[46]. Although ZigBee wireless technology is able to resolve wired system problems in terms of cost and installation, it operates in the 2.4 GHz ISM radio frequency band in which Wi-Fi wireless technology is employed for

WLAN in buildings. Thus, ZigBee technology may have potential interference issues when operated with Wi-Fi [47-49], which has motivated researchers to study other emerging technologies For example, in [47] the authors have studied the interference between microwave ovens and WiFi transmitters and have concluded that throughput performance can be affected due to this interference. Based on the study in [48], when ZigBee co-exists with WLAN and Bluetooth the dominant interference source is the WLAN.

In this chapter we discuss the design and implementation of a wireless-based LED lighting testbed integrated with light and occupancy sensors. The system utilizes BLE wireless modules, which can be configured to form a network for data exchange between different components including sensors and actuators. Characteristics such as ultra-low power consumption, along with other advantages such as small form factor, low cost, and backward capability, make BLE an attractive technology for wireless sensors in energy-efficient applications. Additionally, BLE uses the adaptive frequency hopping (AFH) technique [50] in order to diminish interference of other wireless technologies and so to achieve reasonable reliability and robustness characteristics. To use the same programming environment tools discussed earlier in Chapter 3, the TI CC2540 SoC was chosen for the BLE-enabled embedded system. The system software comprises a back-end embedded program and a front-end graphical user interface (GUI) to demonstrate the real-time LED dimming level, lighting fixture power consumption, and the state of the motion detector. The experimental setup, consisting of a BLE-enabled ambient light sensor, motion detector, and dimmer circuit along with a 150W high-bay LED fixture is presented in this chapter.

4.1. System Design and Implementation

Figure 4.1 illustrates the developed BLE-enabled energy-efficient lighting system block diagram containing a central system and BLE piconets. The central system consists of a BLE master device and host PC equipped with a graphical user interface. The BLE-enabled ambient light sensor, motion detector, and dimmer, as well as a LED lighting fixture, constitute a BLE piconet. The LED fixture light level is controlled using a

BLE-enabled dimmer that it is programmed by means of a combination of ambient light level and motion detector over-the-air.

Figure 4.1: BLE-enabled energy-efficient lighting system block diagram

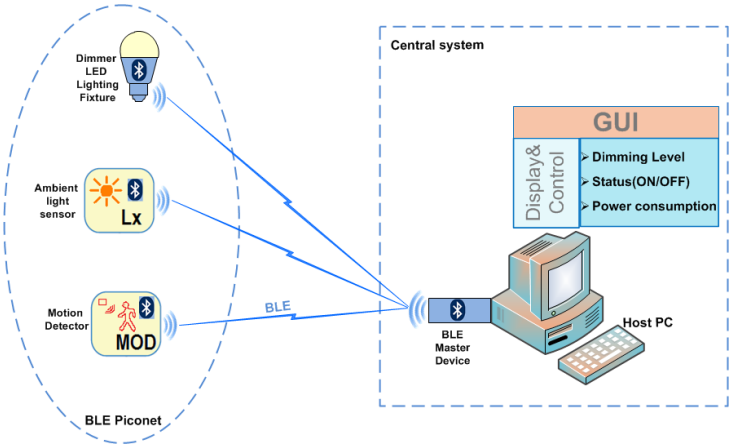

The system is divided into two main components: hardware and software, with each component divided into several modules. The BLE network utilizes a TI CC2540 chip that is a low-cost, low-power, true system-on-chip (SoC) for Bluetooth low energy applications [45]. It enables robust BLE master or slave nodes to be built with very low total bill-of-material costs. The CC2540 combines an excellent RF transceiver with an industry-standard enhanced 8051 MCU. Indeed, CC2540 is the same as CC2530 with the only difference at the RF transceiver stage. Consequently, all development tools such as SmartRF05EB and IAR that were utilized for CC2530 in Chapter 3 are applicable for CC2540 by considering the BLE stack protocol instead of ZigBee. The CC2540 Mini Development Kit [45] is utilized to avoid time spent on PCB and circuit fabrication. The kit contains a CC2540 USB Dongle and CC2540 Keyfob that operate as BLE master and slave nodes respectively. The hardware and software are discussed in detail in the following sections.

4.1.1. *Hardware Components*

The piconet constitutes a BLE-enabled ambient light sensor, motion detector, and dimmer, referred to as BLE slave nodes in this work. The CC2540 Keyfob is the main part of these devices and handles the local process for each device and provides

BLE connectivity. On the other side, the central system employs a CC2540 USB dongle as the BLE master device that it is responsible for data exchange between the piconet devices and host PC. Thus, the hardware components considered in the design phase are as follows.

4.1.1.1. TI CC2540 Keyfob

The TI CC2540 Keyfob [45] is a working reference design for software development of single-mode Bluetooth low energy applications based on the TI CC2540. It operates as a BLE peripheral device and contains modifiable software that can be tailored toward different applications. The proposed design considers Keyfob not only to perform the local process for each piconet device but also to be responsible for data exchange with the BLE master device through BLE connectivity. Table 4.1 presents CC2540 IO pins that are accessible on Keyfob header connections. The debug header connection is used for programming and debugging purposes, but the test header connection, in contrast, can be utilized to interface with other devices. The Keyfob power is supplied by a 3.3V coin cell battery for the ambient light sensor and motion detector. However, the dimmer is installed in the LED fixtures where the DC-line is accessible and the dimmer is energized using this line.

Table 4.1: CC2540 IO pins that are accessible on Keyfob header connections

Debug Header pin	IO pin	Functionality	Test Header Pin	IO pin	Functionality
1	-	GND	1	P0_6	IO / ADC
2	-	VDD	2	P1_5	IO / ADC
3	P2_2	DC	3	P0_7	IO / ADC
4	P2_1	DD	4	P1_7	IO / ADC
5	P0_4	SSN	5	P0_1	IO / ADC
6	P0_5	SCK	6	P1_4	IO / ADC
7	-	RESET_N	7	P0_0	IO / ADC
8	P0_3	MOSI	8	P1_3	IO / ADC
9	-	VDD	9	-	-
10	P0_2	MISO	10	P1_2	IO / ADC

4.1.1.2. TI CC2540 USB Dongle

The TI CC2540 USB dongle [51] enables both BLE and USB connectivity that facilitate data exchange between the host PC and piconet devices. It is similar to the CC2531 USB dongle reviewed in Chapter 3, with the exception of the RF transceiver. Therefore, the USB dongle operations that were explained in Section 3.1.1.6 are applicable to the CC2540 USB dongle.

4.1.1.3. BLE-enabled Ambient Light Sensor

An ambient light sensor is used in the daylight harvesting mechanism by employing ambient light level measurement in order to specify the dimming level of the LED lighting. Figure 4.2 illustrates a BLE-enabled ambient light sensor schematic diagram constituting a TI CC2540 Keyfob, Osram SFH3310 phototransistor [52], and an amplifier stage. The SFH3310 is an ambient light silicon NPN phototransistor with V-lambda characteristics and low output current. It is able to measure light intensity 10000lux in the full range (see Appendix F). The transistor Q1 is a single-stage bipolar junction transistor (BJT) amplifier that performs phototransistor output signal conditioning. The amplifier output is connected to pin 6 in IO port 0 (i.e., P0_6) of the CC2540 that operates in the ADC mode. Consequently, the ambient light level is converted to a digital signal that is ready to be sent to the BLE master device.

Figure 4.2: BLE-enabled ambient light sensor schematic

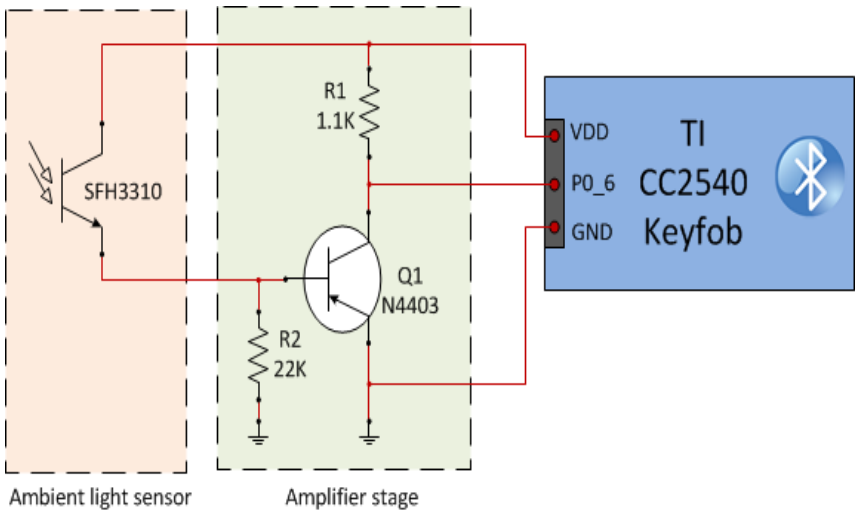

4.1.1.4. BLE-enabled Motion Detector

The motion detector employs a passive infrared (PIR) sensor in order to specify occupancy status. The detector is a Panasonic PIR model EKMB1103113 (see Appendix G) with built-in amplifier and digital output [53] that detects the temperature difference between the detection target and its surroundings. The PIR sensor output connects to an amplifier stage in order to perform signal conditioning and satisfy the next stage input requirements (see Figure 4.3).

Figure 4.3: BLE-enabled motion detector schematic

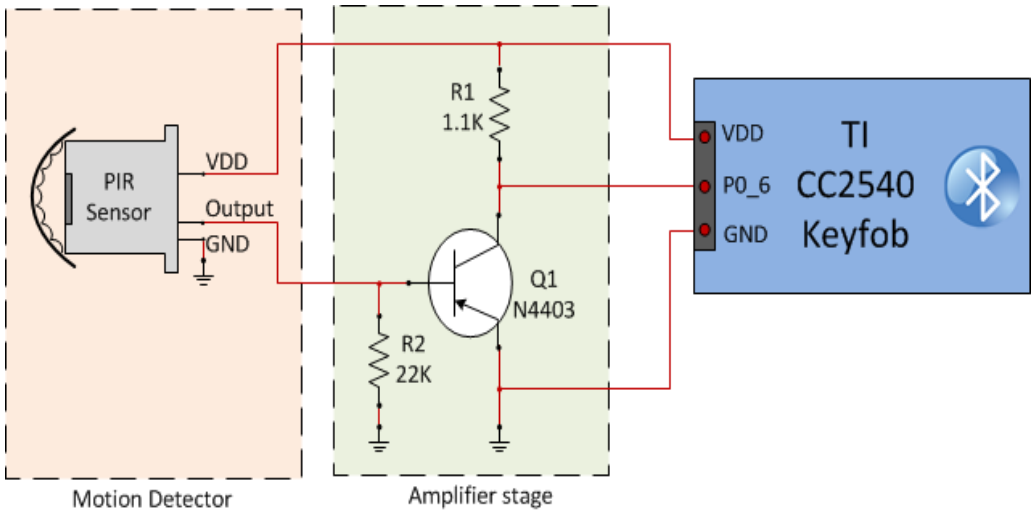

According to the Panasonic PIR sensor's electrical characteristics, its minimum output voltage is VDD-0.5V in detection mode. Figure 4.4 illustrates the PIR sensor timing chart, with the operation divided into three modes as follows:

- **Sleep mode:** When the output is OFF, the electrical current consumption is approximately 1µA.
- **Standby mode:** After the sensor output reaches ON status, the sensor switches to standby mode. The electrical current consumption is approximately 1.9 µA. When the sensor output returns to an OFF state and the hold time expires, the sensor switches to sleep mode.
- **Mask mode:** Time during which the output is forced to OFF after the end of standby mode and consequently detection is not possible during this time.

The motion detector output connects to pin six in IO port zero (i.e., P0_6) of the CC2540 that is operating in the input mode.

Figure 4.4: PIR sensor timing chart

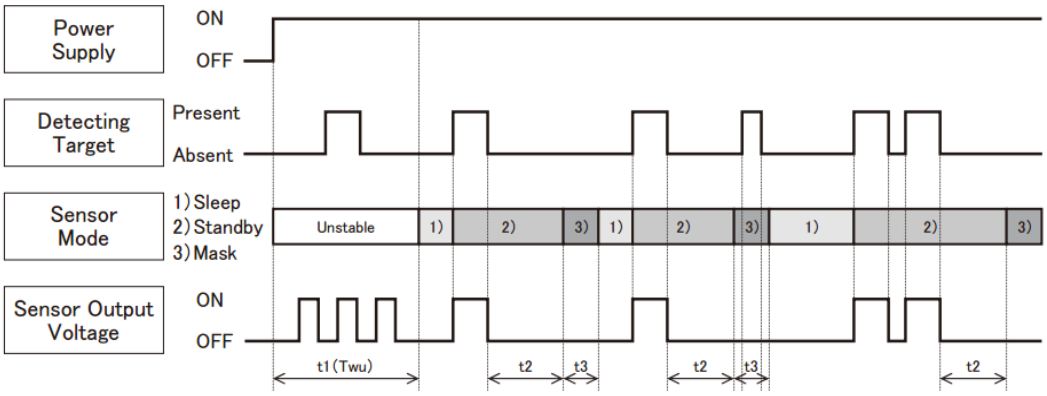

4.1.1.5. BLE-enabled Dimmer

Energy efficiency is accomplished in LED lighting by means of a dimming mechanism according to the combination of daylight harvesting and occupancy status. In this design, pulse-width modulation (PWM) dimming is considered owing to its simplicity of implementation with LED lighting; however, other techniques such as analog and phase control dimming are applicable. In PWM dimming, the LEDs are driven with full amplitude pulses of current and the width of the pulses is varied to control the apparent brightness. This type of dimming relies on the capability of the human eye to integrate the average amount of light in the pulses. Figure 4.5 illustrates a BLE-enabled dimming schematic based on the PWM dimming technique. The TI CC2540 produces the PWM signal and transfers it to the PWM switch through IO pin P1_7 that operates in peripheral mode. The PWM switch constitutes Q1 MOSFET model IRFP260 [54] that benefits from fast switching, low on-resistance and cost-effective features (see Appendix H).

Figure 4.5: BLE-enabled dimmer schematic

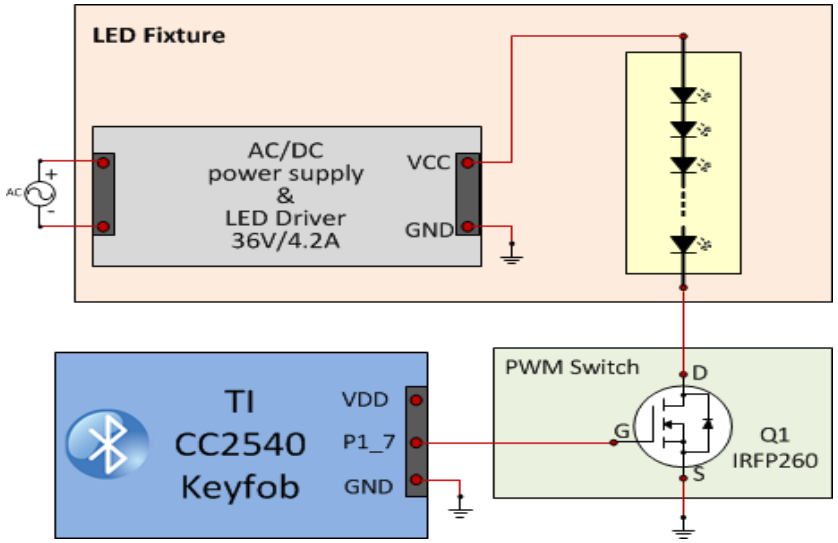

The BLE master device sends both ambient light level and occupancy status to the BLE-enabled dimmer. The Keyfob, in the dimmer, is not only responsible for receiving that data and calculating the dimming level but also resolves the duty cycle and produces the PWM signal. Subsequently, the PWM signal switches ON/OFF Q1 through the MOSFT gate and decreases the forward bias current of the LED string that dims the LED light intensity. Indeed, this mechanism cuts the supply of current for short intervals, thereby causing the LED to turn OFF, but before the light turns completely OFF, the current supply is established. Considering the switching frequency in the range of hundreds, the human eye perceives the LED lighting as dimmed.

4.1.2. *Software Design and Development*

The software consists of back-end embedded programs that are implemented on the embedded platforms (i.e., TI CC2540 SoC) and the front-end graphical user interface running on the host PC. The back-end embedded software is programmed by C code, taking advantage of the TI Bluetooth low energy software stack [26], and was developed by means of the IAR Embedded Workbench integrated development environment (IDE). This IDE tool supports compiling and debugging of the CC25xx SoC family through the SmartRF05EB. Moreover, it is bundled with all the files required for CC25xx to start

development, such as register definition, header files, linker command files, driver, and device description files needed for debugging and programming.

According to the Bluetooth low energy network topology, the ambient light sensor, motion detector, and dimmer (i.e., piconet devices) operate in slave and server roles in the link and ATT layers respectively. On the other hand, the CC2540 USB dongle performs master and client roles in these layers. Additionally, the TI BLE software platform supports two different stack configurations for the BLE devices as follows [26]:

- **Single-Device:** The controller, host, profiles, and application are implemented on the CC254x as a true single chip solution.
- **Network Processor:** The controller and host are implemented together on the CC254x while the profiles and application are implemented separately. The application and profiles communicate with the CC254x by means of vendor-specific HCI commands using a hardware or UART interface, or using a virtual UART interface over USB.

The BLE-enabled ambient light sensor, motion detector, and dimmer were designed and developed in single-device configuration and the BLE master device that interfaces with the host PC is implemented in network processor configuration. In addition to the roles and configuration, the BLE application requires some software profiles performed in the BLE software stack or developed by Bluetooth low energy software developers. However, the energy-efficient lighting profiles utilized in this research consist of ambient light, motion detector, and dimmer profiles developed for the first time.

4.1.2.1. Ambient Light Sensor Software Development

The ambient light sensor software contains the ambient light profile and is responsible for reading the ambient light level and transferring it to the BLE master device through the BLE connection. The ambient light level is a hexadecimal number in the range 0x0000 to 0x2710 that represents light intensity between 0 lux and 10,000 lux (i.e., SFH310 phototransistor operation range). Figure 4.6 illustrates the ambient light sensor operation starting with system initialization and a non-stop loop handled by the

operating system abstract layer (OSAL). The OSAL is not an actual operating system (OS) in the traditional sense, but rather a control loop that allows the software to set up the execution of events [26].

The ambient light sensor functionality can be modeled using a state machine by taking such roles as slave and server in the connection preparation state. After the connection preparation phase, the state machine changes to the advertising mode and remains in this state until connection is established. Next, it transfers to a continuance ambient light level measurement situation that is a simple ADC read process. The state changes to read response, whereupon a BLE read request arrives from the BLE master device and returns to the previous state immediately after performing read response. Both read ambient light and read response states occur in the connection mode. If, for any reason, disconnection occurs in these steps, the state automatically transfers to the advertising mode.

Figure 4.6: Ambient light sensor operation state machine

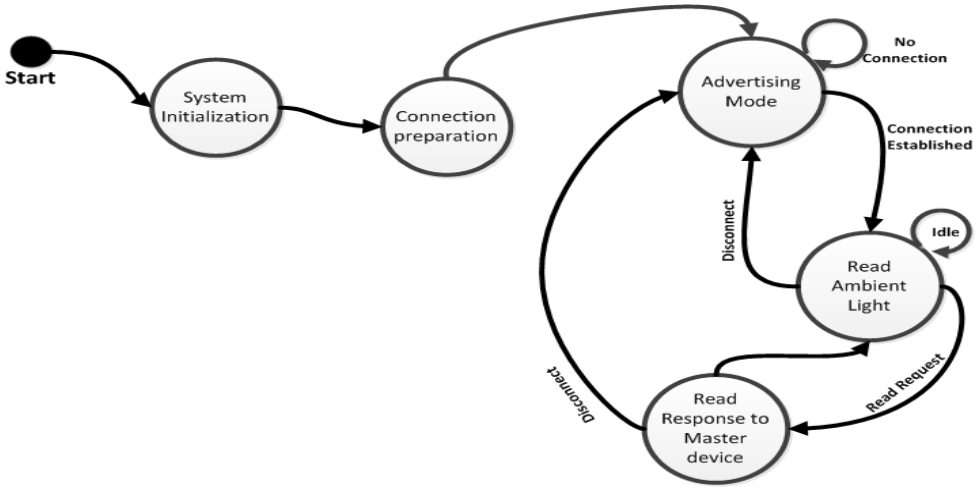

4.1.2.2. Motion Detector Software Development

The motion detector software contains a motion detector profile that is responsible for determining occupancy status and transferring it to the BLE master device through BLE connectivity. The occupancy status can be 0x8000 or 0x0000 to represent existing and non-existing occupant conditions respectively. Figure 4.7 illustrates the operation of the motion detector state machine. This software is the same

as the ambient light sensor, except for reading the occupancy status state, which is a simple logic level detection.

Figure 4.7: Motion detector operation state machine

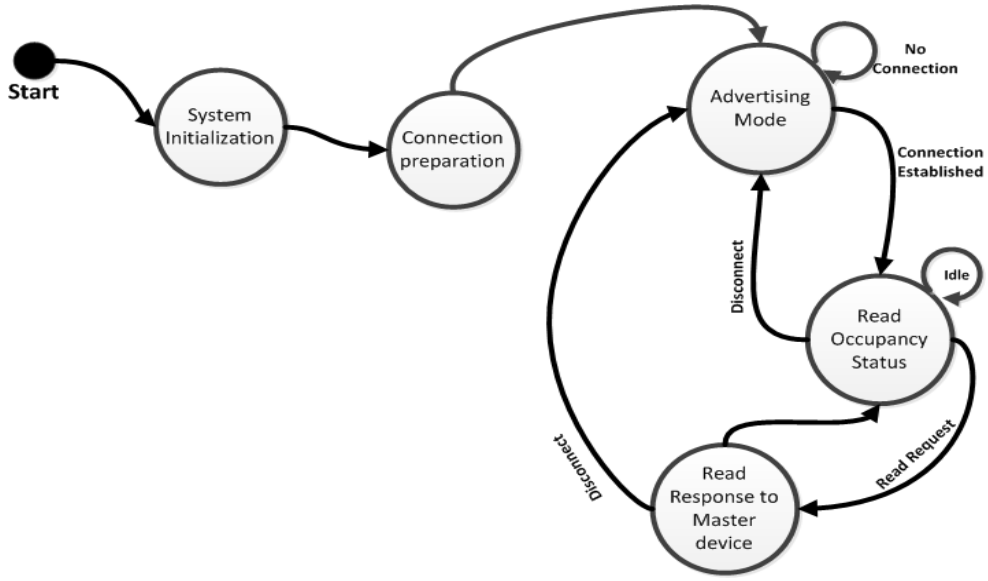

4.1.2.3. Dimmer Software Development

The dimmer software is more complex in comparison with the previous case as the dimmer profile needs to manage the system timer to generate the PWM signal. The dimming level is a logical OR operation of ambient light level and occupancy status that can be a hexadecimal number between 0x0000 and 0xA710. The BLE master device utilizes logical OR operation to send dimming data in one cycle. TI CC2540 is equipped with four independent programmable timers[10] with timer/counter/PWM functionality. In this design, a 300Hz PWM signal is generated by means of timer 3 that can produce the required duty cycle for the LED lighting dimmer.

[10] They contain two 16-bits (i.e., timer 1 and 2) and two 8-bits (i.e., timer 3 and 4) timers. Note that Timer 2 is for timekeeping in the BLE link layer and it must not be used by any application.

Figure 4.8: Dimmer operation state machine

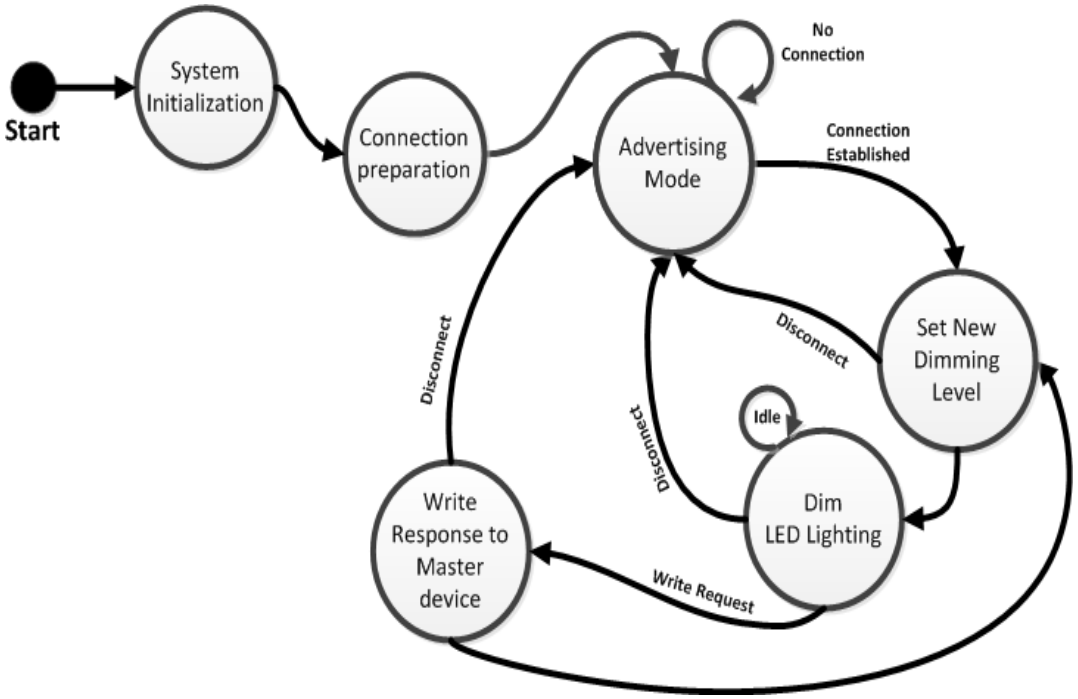

According to the dimmer profile algorithm, the state machine will set a new dimming level after connection is established (see Figure 4.8). In this phase, the PWM duty cycle is computed in accordance with the ambient light level and occupancy status that come from the BLE master device. Next, in the dim LED lighting state, the PWM signal is generated using timer 3 and the system will remain in this stage until a write command is requested from the BLE master device. This is the step in which new parameters (i.e., ambient light level and occupancy status) are received and the system state is transferred to a new dimming level. Again, if disconnection occurs, the state changes to the advertising mode.

4.1.2.4. BLE Master Device Software Development

The BLE master device is responsible for receiving ambient light level and occupancy status and sending them to the dimmer by means of the ATT read and write requests, respectively. It acts as a master node in the BLE network topology, while also sending request commands to piconet devices, and consequently operates as a client in

the ATT layer. Additionally, it interfaces with the host PC and should be configured as a network processor.

Figure 4.9: BLE master device operation state machine

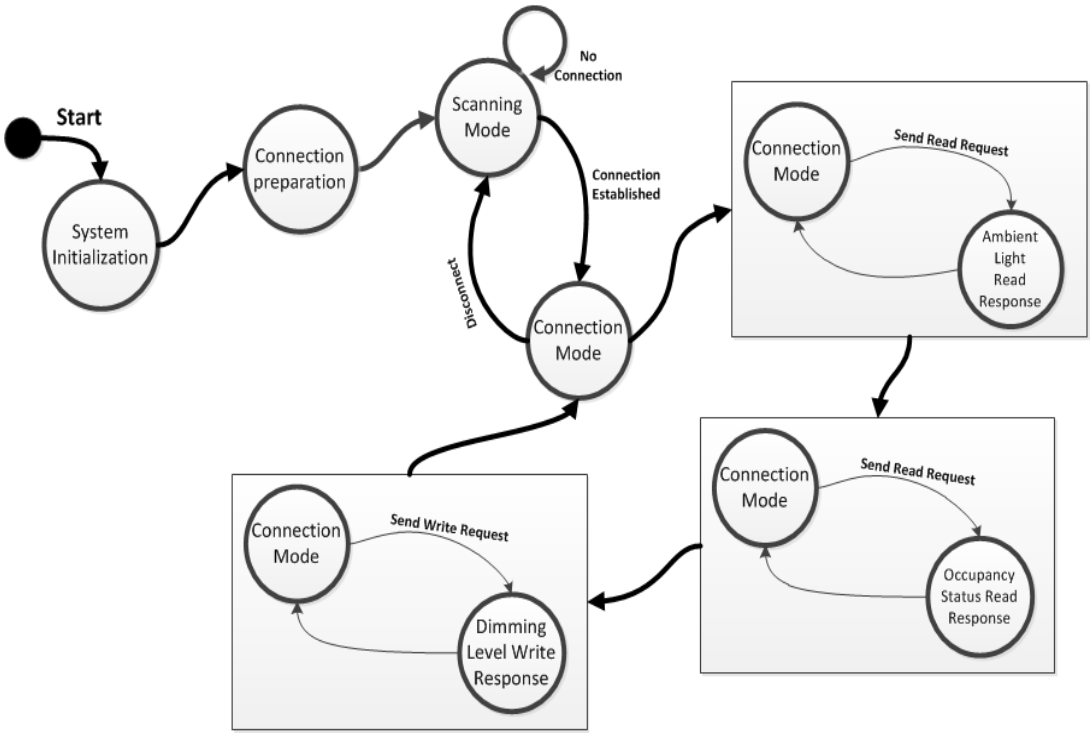

Figure 4.9 represents how the BLE master device interacts with other devices. After system initialization and connection preparation, the scanning mode state begins and the BLE master device attempts to connect to piconet devices. In the connection state, there are three sequential processes consisting of the ambient light ATT read request, occupancy status ATT read request, and dimming level ATT write request. Correspondingly, three response states are defined for these request commands. In the case of disconnection, the state changes to scanning mode and the BLE master device attempts to establish a new connection.

4.1.2.5. GUI Software Development

The graphical user interface provides users with monitoring and control facilities in order to manage lighting power consumption. The GUI is developed by the NI LabView programming environment and consists of display and control panels (see

Figure 4.10). It runs on a host PC and interfaces with the BLE network through serial to USB virtual port.

Figure 4.10: Graphical user interface

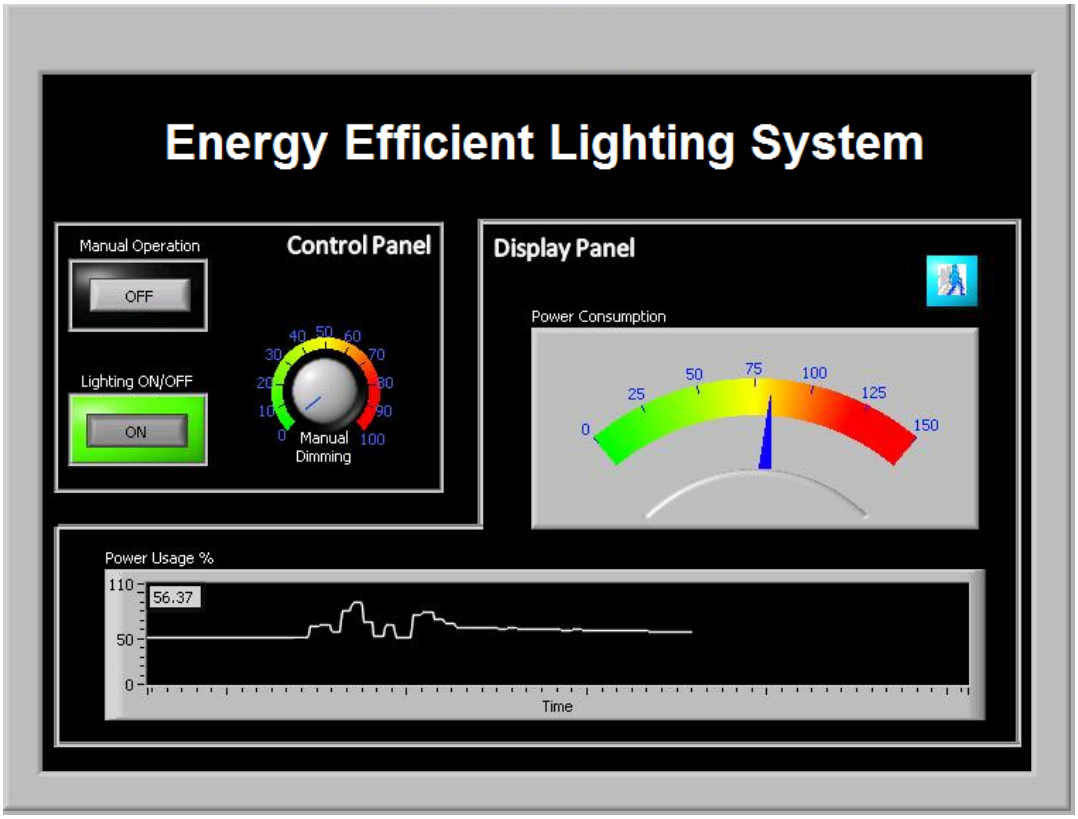

The display panel demonstrates run-time power consumption, the percentage of the power usage, and occupancy status. The control panel facilitates manual operations including LED lighting ON/OFF controls and manual dimming. Indeed, the control panel grants the user permission to override automatic operation. Figure 4.11 illustrates a GUI operation state machine that begins by serial port initialization. Depending on the mode of operation, automatic or manual, it transfers to the next state. In the automatic operation mode, each second the state changes to the read and display process during which the power consumption, percentage of power usage, and occupancy status are read and displayed. However, that data is overridden in the manual operation, depending on the user's decision.

Figure 4.11 GUI operation state machine

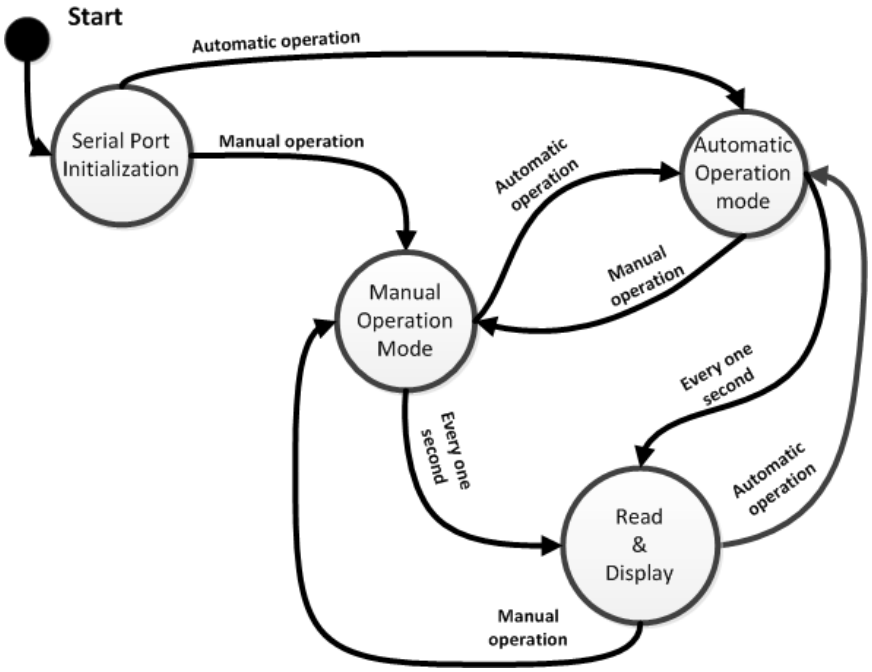

4.2. System Integration and Experimental Evaluation

The hardware components were individually designed and implemented, and corresponding software for these components was developed as a part of the thesis work performed. The proof-of-concept energy-efficient lighting system was investigated by means of the experimental setup comprising a BLE-enabled ambient light sensor, motion detector, LED dimmer circuits, a USB dongle, a high-power 150W LED lighting fixture, and a host PC equipped with GUI (see Figure 4.12). This testbed is located in the Motion and Power Electronics Control Lab at SFU. The BLE-enabled ambient light sensor is placed in front of a window and away from the LED fixture. Moreover, the BLE-enabled motion detector is installed in a appropriate position where it is able to recognize the presence of occupants.

Figure 4.12: Experimental setup for energy-efficient intelligent lighting system using BLE

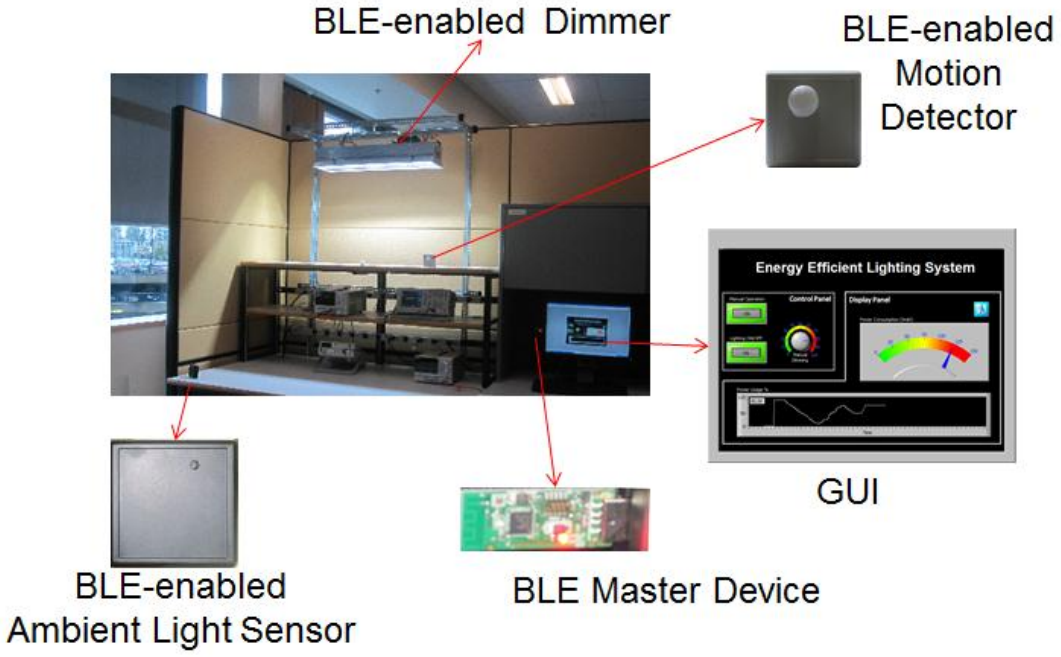

The experiment begins with automatic mode and an unoccupied condition with the curtains down to prevent daylight from entering the lab. Consequently, the LED lighting fixture is in the OFF state and power consumption shows a value around zero (see Figure 4.13.a). Regardless of the ambient light level, the fixture remains OFF pending an occupant or manual turn on. The LED lighting switches to ON with full light level (i.e., non-existing daylight condition) immediately after an occupant is detected (see Figure 4.13.b). In this case, maximum power is consumed and the fixture operates inefficiently. To demonstrate daylight harvesting, the curtains were drawn back to allow sunlight into the room, resulting in an increase in the level of the interior light level. The ambient light sensor measures the new light intensity and transfers it to the dimmer through the BLE connection and the BLE master device. Accordingly, the dimmer reduces the PWM duty cycle, hence dimming the LED lighting level. The above scenario was repeated several times, based on which the power usage percentage chart shown in Figure 4.13.c was obtained. The Figure 4.13.c illustrates how daylight changes the LED fixture power consumption. Indeed, a combination of daylight and artificial light facilitates energy efficiency in the lighting system. Furthermore, the occupant can

manually operate the system by switching ON the system and dim the lighting through the control panel (see Figure 4.13.d).

Figure 4.13: Experimental results for energy-efficient lighting system

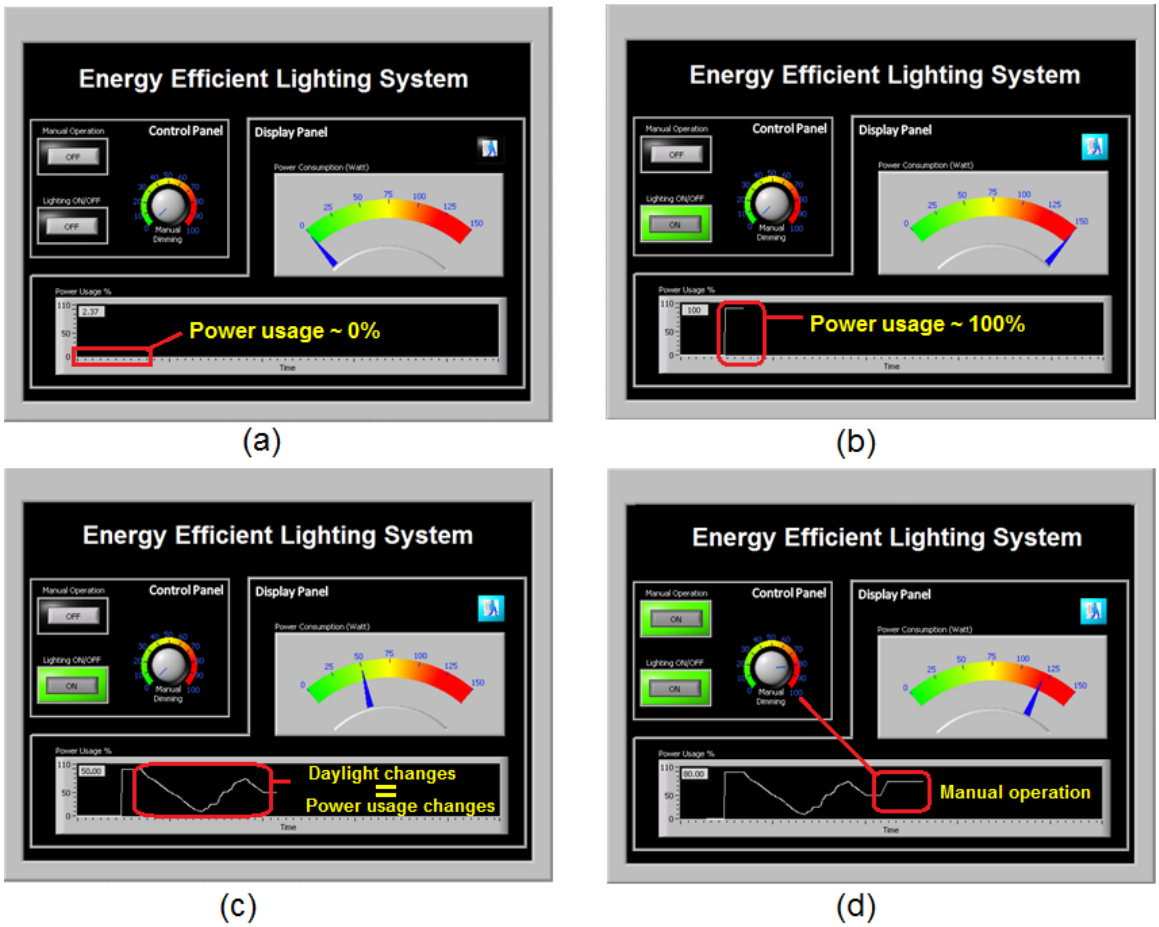

Chapter 5: Concluding Remarks and Directions for Future Research

In this thesis, wireless embedded systems were studied and utilized with two applications to renewable energy and energy efficiency. These applications addressed two solutions for reducing total life cycle costs of solar PV electricity production and decreasing energy consumption in buildings using an energy-efficient lighting system. To investigate the research outcome, proof-of-concept systems consisting of prototype devices and testbeds were implemented. Conclusions and future works for these researches are described in the following.

5.1. PV Module Performance Monitoring System Using ZigBee Technology

Performance monitoring in a solar power plant at PV module level is crucial to reduce the operational and maintenance costs of solar PV power systems. To attain this objective, a controller and monitoring system comprising hardware and software is required. On the other hand, such a system needs data communication for its operation. To avoid the cost of extra wiring, wireless-embedded systems are able to provide alternative solutions. Hence, a ZigBee-enabled system-on-chip was utilized for this purpose because of its advantages in terms of low cost, mesh topology, and low power consumption. According to the experimental results, this system is able to report real-time conditions of PV modules that help to find underperforming PV modules and reduce maintenance costs, and consequently decrease the total life cycle cost. The LCOE factor is not only directly proportional to TLCC but is also in inverse proportion to total lifetime energy production (TLEP). A popular method for increasing the TLEP of the solar PV is maximum power point tracking technique at inverter level [55]-[56], although it has some drawbacks such as mismatch losses between the PV panels, and MPPT power losses as well as block diodes losses [57]. Recently, the MPPT technique at the PV module level has motivated researchers to undertake new research in order to find cost-effective

solutions for this purpose [58]-[59]. However, MPPT at module level requires data communication with a central controller module and this can be accomplished using a wireless system. Thus, the results in this thesis can be utilized in the study of ZigBee-enabled MPPT systems at the PV module level for future research that makes it possible to increase TLEP by maximizing the PV module power output.

5.2. Energy-efficient Lighting Using Bluetooth Low Energy

Utilizing energy-efficient systems leads to decreasing power consumption and energy demand. This strategy makes it possible to perform the same functions with less electricity. This is especially important when the cost of generation of renewable energy is high, as is the case for many sources of renewable energy such as solar, wind, and wave power. To achieve this objective, an energy-efficient LED lighting system was implemented using the Bluetooth low energy technology. The experimental results demonstrate how the power consumption of an LED lighting luminaire can be decreased using BLE-enabled ambient light and occupancy sensors and a dimmer. Although the concept of the energy-efficient lighting system was not new, this is the first time that BLE as an emerging technology has been studied for this purpose. The most important research outcomes are BLE profiles for an energy-efficient lighting system that were designed and developed for the first time. Considering the energy consumption breakdown in commercial buildings (see Figure 1.2), it seems that expanding this technique and acquiring a total solution for energy-efficiency in buildings requires a general energy-efficient BLE profile, consisting of lighting, HVAC, appliances, security, etc., and this is recommended for future work.

Appendices

Appendix A.

TI CC2530 SoC

www.ti.com/sc/device/CC2530

2.4-GHz IEEE 802.15.4/ZigBee®/RF4CE System-on-Chip Solution
CC2530

The CC2530 is a cost-effective, low power, and true system-on-chip solution specifically tailored to IEEE 802.15.4 point to point and star or ZigBee PRO mesh network applications

The CC2530 comes in four different versions: CC2530-F32/64/128/256, with 32/64/128/256-KB flash memory respectively and combines a fully integrated high-performance RF transceiver with an industry-standard enhanced 8051 MCU, 8-KB RAM and other powerful supporting features and peripherals.

Key Features

- Up to 256-kB flash with 20K erase cycles to support over-the-air updates, large applications
- 8-kB RAM for more complex applications and ZigBee profiles
- Programmable output power up to +4.5 dBm
- Less than 1-µA current consumption in power down with sleep timer running
- Includes powerful address recognition and packet processing engine

Benefits

- Supports ZigBee/ZigBee PRO, ZigBee RF4CE, 6LoWPAN, and all 802.15.4-based solutions
- Excellent receiver sensitivity and programmable output power
- Very low current consumption in RX, TX, and multiple low-power modes ensure long battery lifetime
- Best- in- class selectivity and blocking performance, with lowest packet error rate. Suited for battery applications.

Applications

- Smart energy/automated meter reading
- Remote controls
- Home/building automation
- Consumer products
- Industrial control and monitoring

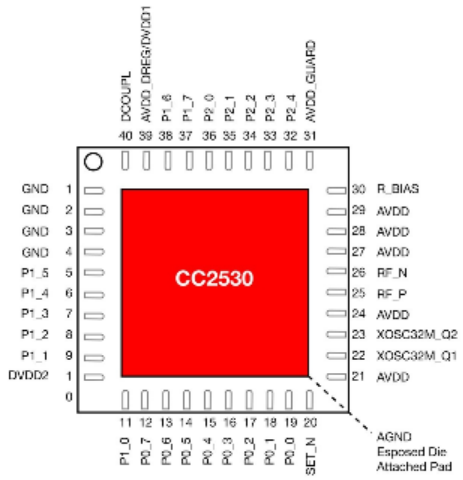

CC2530 block diagram.

General Characteristics

Parameter	Min	Typ	Max	Unit
Operating conditions				
Frequency range	2400	—	2483.6	MHz
Operating temperature range	–40	—	125	°C
Operating supply voltage	2.0	—	3.6	V
Radio bit rate	—	250	—	kBaud
Receiver sensitivity	—	–97	—	dBm
Adjacent channel rejection	—	49/49	—	dB
Alternate channel rejection	—	57/57	—	dB
Blocking	—	57/57	—	dB
Nominal output power in TX mode	—	+4.5	—	dBm
Current consumption				
MCU active and RX mode	—	25	—	mA
MCU active and TX mode, +4 dBm	—	34	—	mA
Power mode 1	—	105	—	µA
Power mode 2	—	1	—	µA
Power mode 3	—	0.4	—	µA
Wake-up and timing				
From power mode 2 or 3 to active	—	120	—	µs
From active to RX or TX	—	192	—	µs

CC2530ZNP

ZigBee® Network Processor
CC2530ZNP

The CC2530ZNP (ZigBee Network Processor) is a low cost and effective way to design with the ZigBee protocol, without having to learn the complexities of the full ZigBee PRO stack and public application profiles. It is recommended for application developers that want to use their existing host processor, or prefer to use another processor to run other applications, while using the CC2530ZNP to communicate with other ZigBee devices. The ZNP is a CC2530 System-on-Chip preloaded with the ZigBee PRO stack, without ZigBee Cluster Library. The CC2530ZNP communicates to the host processor via an SPI or UART command interface. The host processor communicates with the ZigBee processor using an easy to use protocol.

Key Features

- Easy to use ZigBee processor (8051 core)
- Integrated ZigBee Pro compliant stack
- Supports the TI Z-Stack™ software and Simple API
- Certified golden platform used in ZigBee interoperability test events
- Best in class selectivity, good coexistence with Wi-Fi® and *Bluetooth*® devices
- Low power consumption

Benefits

- Integrated HW design shortens time to market by 25%
- Embedded stack with simple sample applications reduce firmware development by up to 50%
- Compact radio reference design makes it ideal for small form factor end devices and sensors
- Low current consumption optimized for sleeping end nodes and battery operated devices

Applications

- Home and building automation
- Industrial monitoring and control
- Sensor networks
- Medical telehealth

Development Tools and Software

- CC2530ZNP-mini kit
- Simple ZigBee applications: Coordinator, router, end-device
- RF tester application: Eases FCC/ETSI testing

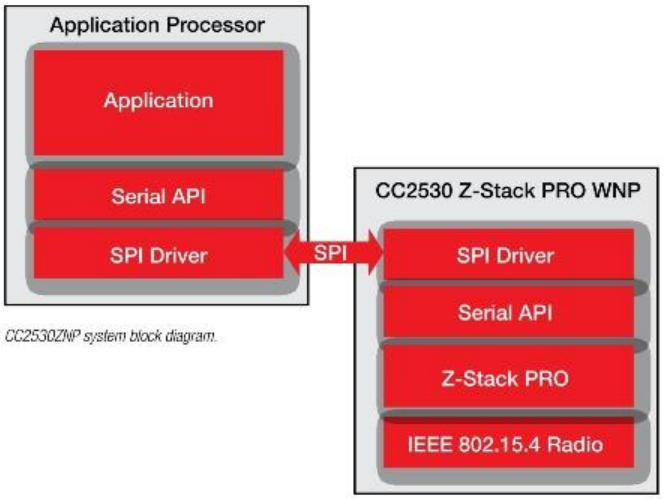

CC2530ZNP system block diagram.

General Characteristics

Parameter	Min	Typ	Max	Unit
Operating conditions				
Frequency range	2400	—	2483.6	MHz
Operating temperature range	–40	—	125	°C
Operating supply voltage	2.0	—	3.6	V
Radio bit rate	—	250	—	kBaud
Receiver sensitivity	—	–97	—	dBm
Adjacent channel rejection	—	49/49	—	dB
Alternate channel rejection	—	57/57	—	dB
Blocking	—	57/57	—	dB
Nominal output power in TX mode	—	+4.5	—	dBm
Current consumption				
MCU active and RX mode	—	25	—	mA
MCU active and TX mode, +4 dBm	—	34	—	mA
Power mode 1	—	105	—	µA
Power mode 2	—	1	—	µA
Power mode 3	—	0.4	—	µA
Wake-up and timing				
From power mode 2 or 3 to active	—	120	—	µs
From active to RX or TX	—	192	—	µs

Appendix B.

MAX4080/MAX4081

76V, High-Side, Current-Sense Amplifiers with Voltage Output

General Description

The MAX4080/MAX4081 are high-side, current-sense amplifiers with an input voltage range that extends from 4.5V to 76V making them ideal for telecom, automotive, backplane, and other systems where high-voltage current monitoring is critical. The MAX4080 is designed for unidirectional current-sense applications and the MAX4081 allows bidirectional current sensing. The MAX4081 single output pin continuously monitors the transition from charge to discharge and avoids the need for a separate polarity output. The MAX4081 requires an external reference to set the zero-current output level (V_{SENSE} = 0V). The charging current is represented by an output voltage from V_{REF} to V_{CC}, while discharge current is given from V_{REF} to GND.

For maximum versatility, the 76V input voltage range applies independently to both supply voltage (V_{CC}) and common-mode input voltage (V_{RS+}). High-side current monitoring does not interfere with the ground path of the load being measured, making the MAX4080/MAX4081 particularly useful in a wide range of high-voltage systems.

The combination of three gain versions (5V/V, 20V/V, 60V/V = F, T, S suffix) and a user-selectable, external sense resistor sets the full-scale current reading and its proportional output voltage. The MAX4080/MAX4081 offer a high level of integration, resulting in a simple, accurate, and compact current-sense solution.

The MAX4080/MAX4081 operate from a 4.5V to 76V single supply and draw only 75µA of supply current. These devices are specified over the automotive operating temperature range (-40°C to +125°C) and are available in a space-saving 8-pin µMAX or SO package.

Applications

Automotive (12V, 24V, or 42V Batteries)

48V Telecom and Backplane Current Measurement

Bidirectional Motor Control

Power-Management Systems

Avalanche Photodiode and PIN-Diode Current Monitoring

General System/Board-Level Current Sensing

Precision High-Voltage Current Sources

Features

- **Wide 4.5V to 76V Input Common-Mode Range**
- **Bidirectional or Unidirectional I_{SENSE}**
- **Low-Cost, Compact, Current-Sense Solution**
- **Three Gain Versions Available**
  - **5V/V (MAX4080F/MAX4081F)**
  - **20V/V (MAX4080T/MAX4081T)**
  - **60V/V (MAX4080S/MAX4081S)**
- **±0.1% Full-Scale Accuracy**
- **Low 100µV Input Offset Voltage**
- **Independent Operating Supply Voltage**
- **75µA Supply Current (MAX4080)**
- **Reference Input for Bidirectional OUT (MAX4081)**
- **Available in a Space-Saving 8-Pin µMAX Package**

Ordering Information

PART	TEMP RANGE	PIN-PACKAGE
MAX4080FAUA	-40°C to +125°C	8 µMAX
MAX4080FASA	-40°C to +125°C	8 SO
MAX4080TAUA	-40°C to +125°C	8 µMAX
MAX4080TASA	-40°C to +125°C	8 SO
MAX4080SAUA	-40°C to +125°C	8 µMAX
MAX4080SASA	-40°C to +125°C	8 SO
MAX4081FAUA	-40°C to +125°C	8 µMAX
MAX4081FASA	-40°C to +125°C	8 SO
MAX4081TAUA	-40°C to +125°C	8 µMAX
MAX4081TASA	-40°C to +125°C	8 SO
MAX4081SAUA	-40°C to +125°C	8 µMAX
MAX4081SASA	-40°C to +125°C	8 SO

Pin Configurations

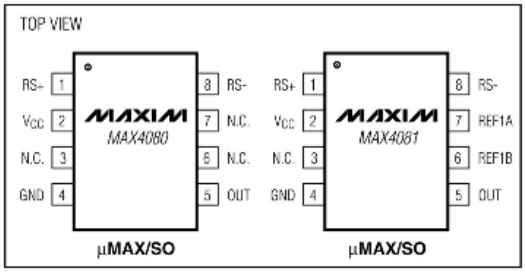

Appendix C.

MAX5033D

500mA, 76V, High-Efficiency, MAXPower Step-Down DC-DC Converter

General Description

The MAX5033 easy-to-use, high-efficiency, high-voltage, step-down DC-DC converter operates from an input voltage up to 76V and consumes only 270µA quiescent current at no load. This pulse-width modulated (PWM) converter operates at a fixed 125kHz switching frequency at heavy loads, and automatically switches to pulse-skipping mode to provide low quiescent current and high efficiency at light loads. The MAX5033 includes internal frequency compensation simplifying circuit implementation. The device uses an internal low-on-resistance, high-voltage, DMOS transistor to obtain high efficiency and reduce overall system cost. This device includes undervoltage lockout, cycle-by-cycle current limit, hiccup-mode output short-circuit protection, and thermal shutdown.

The MAX5033 delivers up to 500mA output current. The output current may be limited by the maximum power dissipation capability of the package. External shutdown is included, featuring 10µA (typ) shutdown current. The MAX5033A/B/C versions have fixed output voltages of 3.3V, 5V, and 12V, respectively, while the MAX5033D features an adjustable output voltage, from 1.25V to 13.2V.

The MAX5033 is available in space-saving 8-pin SO and 8-pin plastic DIP packages and operates over the automotive (-40°C to +125°C) temperature range.

Applications

Automotive

Consumer Electronics

Industrial

Distributed Power

Typical Operating Circuit

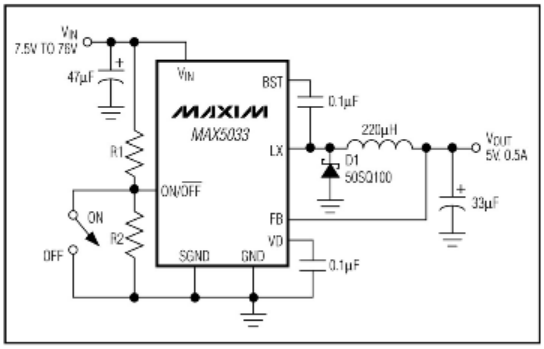

Features

- **Wide 7.5V to 76V Input Voltage Range**
- **Fixed (3.3V, 5V, 12V) and Adjustable (1.25V to 13.2V) Voltage Versions**
- **500mA Output Current**
- **Efficiency Up to 94%**
- **Internal 0.4Ω High-Side DMOS FET**
- **270µA Quiescent Current at No Load, 10µA Shutdown Current**
- **Internal Frequency Compensation**
- **Fixed 125kHz Switching Frequency**
- **Thermal Shutdown and Short-Circuit Current Limit**
- **8-Pin SO and PDIP Packages**

Ordering Information

PART	TEMP RANGE	PIN-PACKAGE	OUTPUT VOLTAGE (V)
MAX5033AUSA	0°C to +85°C	8 SO	3.3
MAX5033AUPA	0°C to +85°C	8 PDIP	
MAX5033AASA	-40°C to +125°C	8 SO	
MAX5033BUSA	0°C to +85°C	8 SO	5.0
MAX5033BUPA	0°C to +85°C	8 PDIP	
MAX5033BASA	-40°C to +125°C	8 SO	
MAX5033CUSA	0°C to +85°C	8 SO	12
MAX5033CUPA	0°C to +85°C	8 PDIP	
MAX5033CASA	-40°C to +125°C	8 SO	
MAX5033DUSA	0°C to +85°C	8 SO	ADJ
MAX5033DUPA	0°C to +85°C	8 PDIP	
MAX5033DASA	-40°C to +125°C	8 SO	

Pin Configuration

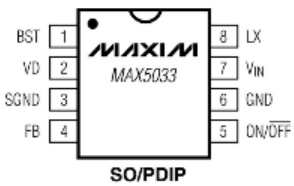

SO/PDIP

Appendix D.
Software C code for ZigBee-enabled solar PV power performance monitoring

D.1. End device source codes

```
/*****************************************************************************

 Filename:              rf_modem_CC2530.c

 Description:           RF Modem cc2530 is an application which reads the voltage and
                        current of PV module and sends them to coordinator through the
                        Zigbee radio between CC2530EM and CC2531 USB Dongle.
                        This application implements a simple ACK handshake on top of
                        MRFI.
 By:                    Younes Rashidi
 Supervised by:         Prof. M. Moallem
 Simon Fraser University/School of Eng. Sc./Mechatronic Systems Eng.
*****************************************************************************/

//-------------------- Includes ---- ----------------------------------------//
#include "hal_defs.h"
#include "../common/mrfi_link.h"
#include "hal_board.h"
#include "hal_mcu.h"
#include "hal_uart.h"
#include "hal_lcd.h"
#include "hal_led.h"
#include "hal_timer_32k.h"
#include "hal_assert.h"
#include "adc.h"
#include "../common/cc8051/adc.h"
#include "util_lcd.h"
#include "stdio.h"
#include "string.h"
#include "math.h"
//-----------------------------------------------------------------------------//

/*****************************************************************************
* CONSTANTS and DEFINITIONS
*/
//------------------------- define application parameters----------------------//
#define APP_PAYLOAD_LENGTH     11
#define DEVICE_1_ADDR       0x25EB
#define DEVICE_2_ADDR       0x25DE
#define MRFI_CHANNEL            0
#define DEVICE_1                0
#define DEVICE_2                1
#define N_RETRIES               5
//-----------------------------------------------------------------------------//


//----------------------- Globale variables ---------------------------------//
static XDATA uint8 pTxData[APP_PAYLOAD_LENGTH];
static XDATA uint8 pRxData[APP_PAYLOAD_LENGTH];
static uint16 appRemoteAddr;
static uint16 appLocalAddr;
static void appRfReceiverTask(void);
```

```
static void appRfSenderTask(void);
uint8  SendOk;
//-------------------------------------------------------------------------------//


//------------------------------- Main Function--------------------------------//
void main(void)
{

 halBoardInit();                                        // Initialise board peripherals.


   while(TRUE) {                                        // Endless loop.
    HAL_PROCESS();                                        // On-board device processing (UART etc.).

    appLocalAddr = DEVICE_2_ADDR;                               // Set local address for End Device.
    appRemoteAddr= DEVICE_1_ADDR;                                 // Set remote address for coordinator.

    mrfiLinkInit(appLocalAddr,appRemoteAddr,MRFI_CHANNEL);              // Initialise the MRFI layer. Selects RF channel
and addresses.

    halTimer32kIntEnable();                                 // Enable 32KHz timer interrupt.


    appRfReceiverTask();                                    // Function for receiving data other End Devices (router role).
    appRfSenderTask();                                      // Function for read voltage/current of PV module and sending them to
coordinator.

    if(SendOk==0x01){                       // If end device could not send packets to coordinator, it try send them to router (mesh
topology).
              appLocalAddr = 0x25DF;                            // Set local address for End Device.
              appRemoteAddr= 0x25EC;                              // Set remote address for router.
              mrfiLinkInit(appLocalAddr,appRemoteAddr,MRFI_CHANNEL);     // Initialise the MRFI layer. Selects RF channel
and addresses.

              appRfSenderTask();                            // function for read voltage/current of PV module and sending them t
router.

              SendOk=0;                                 // Clear sending flag for next loop.
                }


            }
}
//------------------------------End of Main Function -------------------------//


//----------- Function for receiving data from coordinator or router----------//
static void appRfReceiverTask(void)
{

 uint16 l;
 uint8 Rf_Ready=0x00;
 appLocalAddr = 0x25EC;
 appRemoteAddr= 0x25DF;


   mrfiLinkInit(appLocalAddr,appRemoteAddr,MRFI_CHANNEL);              // Initialise the MRFI layer. Selects RF channel
and addresses.

   halTimer32kIntEnable();                                 // Enable 32KHz timer interrupt.


    for(l=0;l<65350;l++){                                 //This loop creates a short delay for verifying if RF data is ready.
       Rf_Ready=mrfiLinkDataRdy();                            //Fuction that Returns true if RF data is ready.
         if (Rf_Ready==0x01){ break;}                        //This condition breaks loop as long as RF data will be ready.
```

```
            }

    if (Rf_Ready==0x01){                        //If RF data is ready, read data and put them in the sending variable.

      mrfiLinkRecv(pRxData,0);                  //Function that Read data from the RX buffer.

      pTxData[5]=pRxData[0];                    //Put received data into sending TX buffer.
      pTxData[6]=pRxData[1];
      pTxData[7]=pRxData[2];
      pTxData[8]=pRxData[3];
      pTxData[9]=pRxData[4];
      pTxData[10]=0x01;                         //Define End Device ID (ID=0,1,...,255).
            }

    else{                                       //If RF data is not ready, clear sending TX buffer.
      pTxData[6]=0;
      pTxData[7]=0;
      pTxData[8]=0;
      pTxData[9]=0;
      pTxData[10]=0;
      }

    Rf_Ready=0x00;                              // clear RF data ready flag for next loop.

}
//---------------------- End of receiving  function ----------------------------//


//----------- Function for read voltage/current of PV module and -------------//
//----------------- sending them to coordinator or router --------------------//
static void appRfSenderTask(void)
{
 uint8 nBytes=0x0B;
 uint8 payloadLength= 0;
 uint8 bytesToRead= 0;


 bytesToRead = MIN(nBytes, APP_PAYLOAD_LENGTH);     // Macro for define number of byte that it should be consider for
the payload
                                                    //length calculation.
  payloadLength+= bytesToRead;                      // calculate payload length.

  pTxData[0]=1;                                   //Define End Device ID (ID=0,1,...,255).

   adcSampleSingle(0x80,0x10, 0x02);                //Function that reads PV module Current from ADC channel 2.
    pTxData[1]=ADCH;                              //Put ADC Data High Byte into sending TX buffer.
    pTxData[2]=ADCL;                              //Put ADC Data low Byte into sending TX buffer.

   adcSampleSingle(0x80,0x10, 0x04);                //Function that reads PV module voltage from ADC channel 4.
    pTxData[3]=ADCH;                              //Put ADC Data High Byte into sending TX buffer.
    pTxData[4]=ADCL;                              //Put ADC Data low Byte into sending TX buffer.

   SendOk=mrfiLinkSend((uint8*)pTxData, payloadLength,N_RETRIES);       //Send data on the RX link.


}
//------------------ End of sending Function ---------------------------------//
```

D.2. Coordinator source codes

```
/*****************************************************************************

 Filename:              rf_modem_CC2531.c

 Description:       RF Modem cc2531 is an application which receives the voltage and
                    current of PV module from End Devices through the Zigbee radio
                    and transmits them to monitoring host computer via USB port.
                    This application implements a simple ACK handshake on top of
                    MRFI.
 By:                 Younes Rashidi
 Supervised by:     Prof. M. Moallem
 Simon Fraser University/School of Eng. Sc./Mechatronic Systems Eng.
*****************************************************************************/

//-------------------  Includes ---- ----------------------------------------//
#include "hal_defs.h"
#include "hal_defs.h"
#include "../common/mrfi_link.h"
#include "hal_board.h"
#include "hal_mcu.h"
#include "hal_uart.h"
#include "hal_lcd.h"
#include "hal_led.h"
#include "hal_timer_32k.h"
#include "hal_assert.h"
#include "util_lcd.h"
#include "stdio.h"
//-----------------------------------------------------------------------------//


/*****************************************************************************
* CONSTANTS and DEFINITIONS
*/
//------------------------- define application parameters---------------------//
#define APP_PAYLOAD_LENGTH      11
#define DEVICE_1_ADDR       0x25EB
#define DEVICE_2_ADDR       0x25DE
#define MRFI_CHANNEL            0
#define INIT                0
#define UART_RX_IDLE_TIME      100
//-----------------------------------------------------------------------------//


//----------------------- Globale variabels ---------------------------------//
static volatile uint8 mrfiPktRdy;
static XDATA uint8 pRxData[APP_PAYLOAD_LENGTH];
static uint16 appRemoteAddr;
static uint16 appLocalAddr;
static volatile uint8 appUartRxIdle;
static void appRfReceiverTask(uint16 Remote_Addr,uint8 remote_num);
static void appConfigTimer(uint16 rate);
//-----------------------------------------------------------------------------//



//------------------------------- Main Function-------------------------------//
void main(void)
{

   appUartRxIdle = FALSE;

    halBoardInit();                                     // Initialise board peripherals.
    halUartInit(HAL_UART_BAUDRATE_38400, 0);                    //Initalise UART. Supported baudrates are: 38400, 57600
and 115200.
```

```
    appConfigTimer(1000/UART_RX_IDLE_TIME);                    //Configure timer interrupts for application. Uses 32 KHz
timer.

      while(TRUE) {                                        // Eldless loop.

       HAL_PROCESS();                                       // On-board device processing (UART etc.).

        appRfReceiverTask(DEVICE_2_ADDR,0);     //receives the voltage and current of PV module from End Devices through
the Zigbee
                                                           //radio and transmits them to monitoring host computer via USB port.
             }
}
//------------------------------End of Main Function -------------------------//

//----------- Function for receiving data from End devices or router----------//
//-------------- and transmits them to monitoring host computer --------------//
static void appRfReceiverTask(uint16 Remote_Addr,uint8 remote_num )
{
 uint8 nToSend;
 uint16 l;
 uint8 Rf_Ready=0x00;

      appLocalAddr = DEVICE_1_ADDR;                        // Set local address for Coordinator.
      appRemoteAddr= DEVICE_2_ADDR;                        // Set remote address for End Device or router.
      mrfiLinkInit(appLocalAddr,appRemoteAddr,MRFI_CHANNEL);          // Initialise the MRFI layer. Selects RF channel
and addresses.

      halTimer32kIntEnable();                              // Enable 32KHz timer interrupt.


      for(l=0;l<65350;l++){                                //This loop creates a short delay for verifying if RF data is ready.
        Rf_Ready=mrfiLinkDataRdy();                        //Fuction that Returns true if RF data is ready.
          if (Rf_Ready==0x01){ break;}                     //This condition breaks loop as long as RF data will be ready.
                }

      halUartEnableRxFlow(FALSE);                          //Signal ready/not ready to receive characters on UART.
      halMcuWaitUs(1000);                                  //Create 1000us delay.

      if (Rf_Ready==0x01){                                 //If RF data is ready, read data and put them in the sending variable.
           nToSend = mrfiLinkRecv(pRxData,remote_num);          //Function that Read data from the RX buffer.
                }

      if(nToSend>0) {                                      ////If number of received data is >0, write  them to  UART.
           halUartWrite(pRxData,nToSend);                  //Write data buffer to UART.
              }


      halUartEnableRxFlow(TRUE);                           //Clear Signal ready/not ready on UART for next loop.

      Rf_Ready=0x00;                                       // clear RF data ready flag for next loop.
}
//---------------------- End of receiving  function ----------------------------//

//------------------------ Interrupt routine function ------------------------//
static void appTimerISR(void)
{
   appUartRxIdle = TRUE;
}
//---------------------- End of Interrupt routine function -------------------//

//---------------------- Connect function to timer interrupt -------------------//
static void appConfigTimer(uint16 rate)
{
   halTimer32kInit(TIMER_32K_CLK_FREQ/rate);
   halTimer32kIntConnect(&appTimerISR);
}
//---------------------- End of Connect function to timer interrupt -----------//
```

Appendix E.

NI LabView code for the PV module performance monitoring GUI

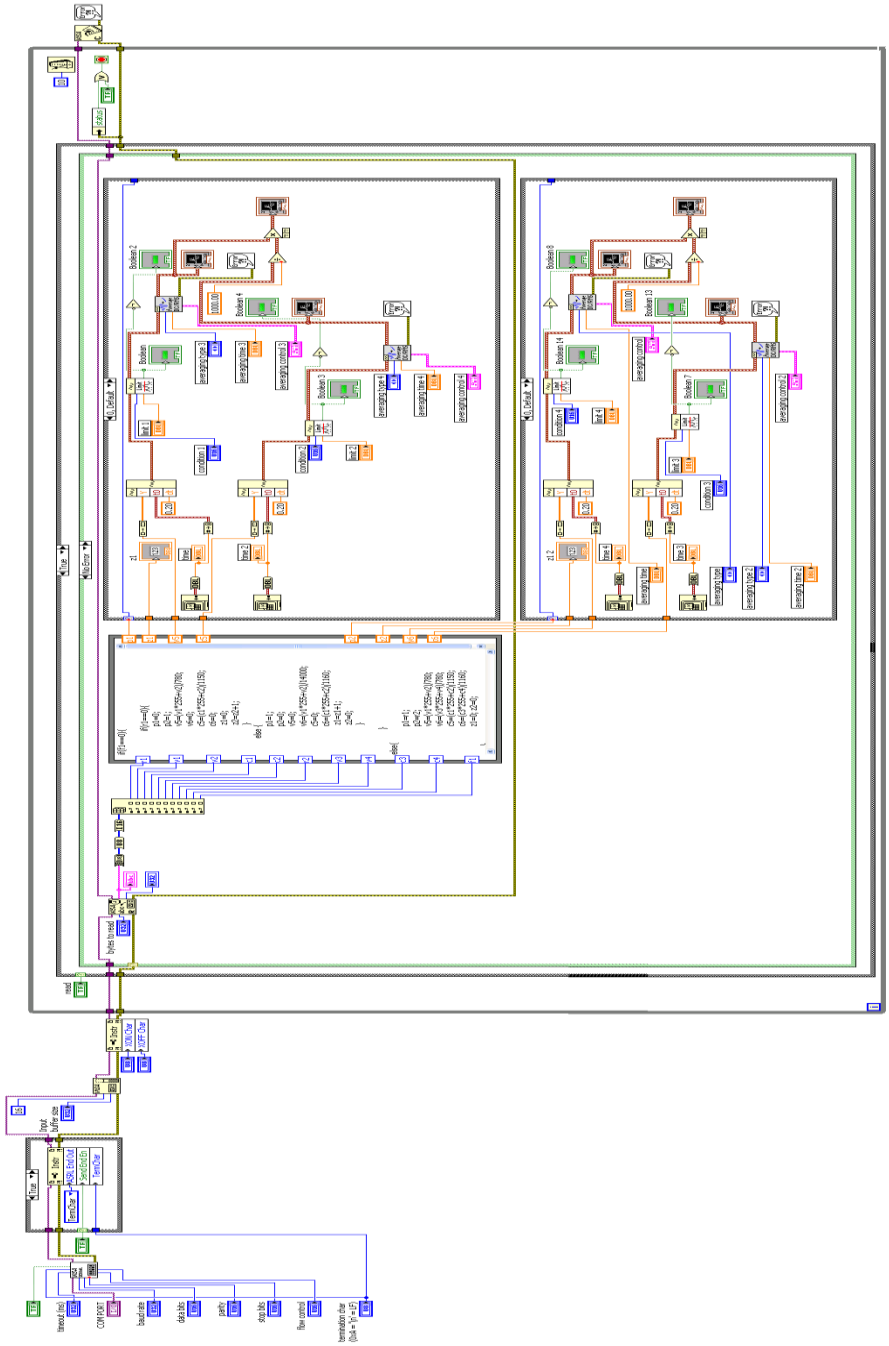

Appendix F.

Phototransistor for ambient sensor

SFH 3310

Wesentliche Merkmale

- Speziell geeignet für Anwendungen im Bereich von 350 nm bis 970 nm
- Angepasst an die Augenempfindlichkeit (V_λ)

Features

- Especially suitable for applications from 350 nm to 970 nm
- Adapted to human eye sensitivity (V_λ)

Anwendungen

- Umgebungslicht-Detektor
- Beleuchtungsmesser
- Dimmungssensor für Hintergrundbeleuchtung
- „Messen/Steuern/Regeln"

Applications

- Ambient light detector
- Exposure meter for daylight and artificial light
- Sensor for Backlight-Dimming
- For control and drive circuits

Typ Type	Bestellnummer Ordering Code	Fotostrom , E_e= 10µW/cm², λ = 560nm, V_{CE} = 5 V Photocurrent Ipce (µA)
SFH 3310	Q65110A5343	2.5...8.0

Grenzwerte (T_A = 25 °C)
Maximum Ratings

Bezeichnung Parameter	Symbol Symbol	Wert Value	Einheit Unit
Betriebs- und Lagertemperatur Operating and storage temperature range	T_{op}; T_{stg}	– 40 … + 100	°C
Kollektor-Emitterspannung Collector-emitter voltage	V_{CE}	5.5	V
Kollektorstrom Collector current	I_C	20	mA
Emitter-Kollektorspannung Emitter-collector voltage	V_{EC}	0.5	V

Kennwerte (T_A = 25 °C)
Characteristics

Bezeichnung Parameter	Symbol Symbol	Wert Value	Einheit Unit
Wellenlänge der max. Fotoempfindlichkeit Wavelength of max. sensitivity	λ_{Smax}	570	nm
Spektraler Bereich der Fotoempfindlichkeit S = 10% von S_{max} Spectral range of sensitivity S = 10% of S_{max}	λ	350 … 970	nm
Bestrahlungsempfindliche Fläche Radiant sensitive area	A	0.29	mm²
Abmessung der Chipfläche Dimensions of chip area	$L \times B$ $L \times W$	0.75 × 0.75	mm × mm
Halbwinkel Half angle	φ	± 75	Grad. deg.
Kapazität, V_{CE} = 0 V, f = 1 MHz, E = 0 Capacitance	C_{CE}	16	pF
Dunkelstrom Dark current V_R = 5 V	I_{CEO}	3 (< 50)	nA

Bezeichnung Parameter	Symbol Symbol	Wert Value		Einheit Unit
		-2	-3	
Fotostrom Photocurrent E_e= 10µW/cm², λ = 560nm, V_{CE} = 5 V E_v = 1000lx, Normlicht/Standard light A	I_{PCE}	2.5…5.0 290	4.0…8.0 460	µA µA
Kollektor-Emitter-Sättigungsspannung Collector-emitter saturation voltage $I_C = I_{PCEmin}$ [1] × 0.3, E_e= 10µW/cm², λ = 560nm	V_{CEsat}	100	100	mV

[1] I_{PCEmin} ist der minimale Fotostrom der jeweiligen Gruppe

[1] I_{PCEmin} is the min. photocurrent of the specified group

Directional Characteristics $S_{rel} = f(\varphi)$

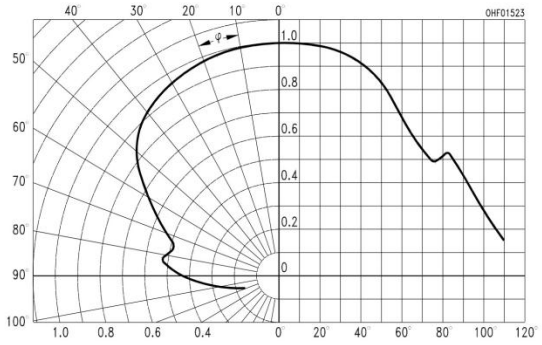

Relative Spectral Sensitivity
$S_{rel} = f(\lambda)$

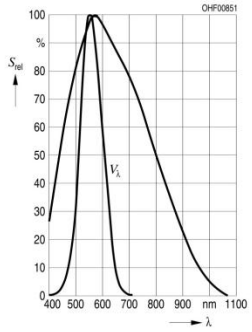

Photocurrent
$I_{PCE} = f(E_V)$, V_{CE} = 5 V

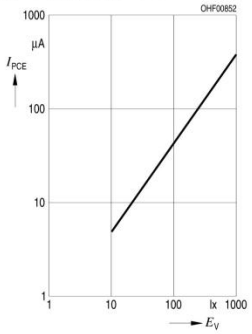

Collector-Emitter Capacitance
$C_{CE} = f(V_{CE})$

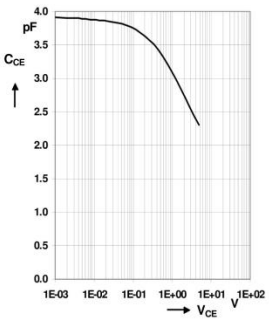

Collector-Emitter Current
$I_{CE} = f(V_{CE}; E_V)$

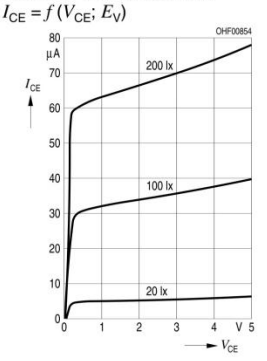

Photocurrent $I_{PCE}/I_{PCE(25\,°C)} = f(T_A)$
E_v = 1000 lx, V_{CE} = 1 V … 5 V

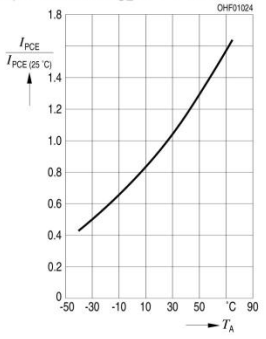

Appendix G.

Passive Infrared Sensor (PIR)

(Standard detection type)

(W) White (B) Black (PW) Pearl White

(Long distance detection type)

(W) White (B) Black (PW) Pearl White

APPLICATIONS

Security Equipment:
- Wireless security sensors, and cameras.

Wireless Devices / Mobile Equipment:
- Wireless occupancy sensors (powered by PV cells or battery)
- PC and smart phone

What is passive infrared type?

This sensor detects changes in infrared radiation which occur when there is movement by a person (or object) which is different in temperature from the surroundings.

① As this sensor detects temperature differences, it is well suited to detecting the motion of people by their body temperature.

② Wide sensing area.

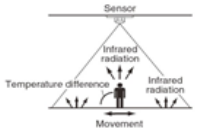

1. *1μA low current consumption with Panasonic's proprietary design*

Development of a specialized circuit allows the reduction of current consumption to 1μA (during sleep mode). When motion is detected, the sensor will shift to "standby" mode.

Reduction of current consumption allows battery life to be extended for battery driven products, including wireless based and low power consumption devices.
(Product lineup includes 1μA, 2μA, and 6μA sensors.)

2. *Simplified circuitry with fully integrated sensor design*

Panasonic's proprietary high-density embedded circuit design eliminates external sensing circuits. Advantages include reduced development and design schedules.

3. *Lead-free pyroelectric elements*

PaPIRs sensing elements contain lithium tantalate and are lead-free. Typical PIR sensing elements are ferroelectric ceramic (PZT) containing lead.

4. *Low curvature lens for product designs*

Panasonic's lens formation technology achieves a semi-flat lens with a smooth surface and minimum protrusion from the device (lens diameter: ϕ9.5mm).

In addition to white and black lens options, pearl white is offered for design aesthetics.
(※Refer to "Dimensions" on page 5)

5. *Robust design prevents false detection*

PaPIRs sensing circuits are enclosed in a metallic can to minimize adverse effects of external electromagnetic fields. Examples include radiated noise caused by cellular phones.

A high S/N ratio minimizes sensitivity to false tripping when operated under various environmental conditions.

Block Diagram *(Digital output circuit)*

Built-in amplifier and comparator connected directly to a microcomputer.

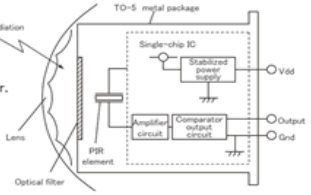

PRODUCT TYPES

Detection Performance	Current Consumption	Lens Color	Model No.	Inner Package	Outer Package
Standard detection type	1μA	White	EKMB1101111	50pcs	1000pcs
		Black	EKMB1101112		
		Pearl White	EKMB1101113		
	2μA	White	EKMB1201111		
		Black	EKMB1201112		
		Pearl White	EKMB1201113		
	6μA	White	EKMB1301111K		
		Black	EKMB1301112K		
		Pearl White	EKMB1301113K		
Long Distance detection type	1μA	White	EKMB1103111	50pcs	1000pcs
		Black	EKMB1103112		
		Pearl White	EKMB1103113		
	2μA	White	EKMB1203111		
		Black	EKMB1203112		
		Pearl White	EKMB1203113		
	6μA	White	EKMB1303111K		
		Black	EKMB1303112K		
		Pearl White	EKMB1303113K		

2. Maximum Rated Values

Items	Specified value
Power Supply Voltage	−0.3～4.5V DC
Usable Ambient Temperature	−20～+60℃ (−4～+140°F) Do not use in a freezing or condensation environment.
Storage Temperature	−20～+70℃ (−4～+158°F)

3. Electrical Characteristic [Measuring conditions: Ambient temperature 25℃(77°F)]

Items		Symbol	1 μA type	2 μA type	6 μA type	Measured Conditions
Operating Voltage	Min.	Vdd	2.3V DC	2.3V DC	2.3V DC	—
	Max.		4.0V DC	4.0V DC	4.0V DC	—
Electrical Current Consumption (Sleep mode) (*4)	Avg.	Iw	1.0 μA	—	—	Iout=0
	Max.		1.6 μA			
Electrical Current Consumption (Standby mode) (*4)	Avg.	Iw	1.9 μA	1.9 μA	6.0 μA	Iout=0
	Max.		3.0 μA	3.0 μA	12.0 μA	
Output Current	Max.	Iout	100 μA	100 μA	100 μA	Vout≧Vdd−0.5
Output Voltage	Min.	Vout	Vdd−0.5VDC	Vdd−0.5VDC	Vdd−0.5VDC	—
Circuit Stability Time (When voltage is applied)	Avg.	Twu	25s	25s	—	—
	Max.		210s	210s	30s	

(*4)(*5) : "Sleep mode" or "Standby mode" is for 1 μA current consumption version.

Digital Output (2 μA and 6 μA current consumption)

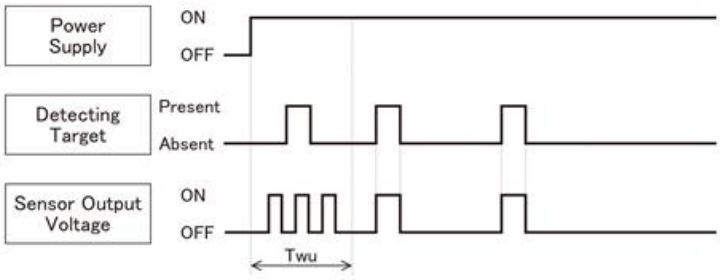

[Durations]

Twu : Circuit Stability Time (2 μA): ~ 25s (typ.)
Circuit Stability Time (6 μA): ~ 30s (max.)
During this stage, output status is undefined (ON/OFF) and detection is not guaranteed.

DETECTION PERFORMANCE

1) Standard detection type

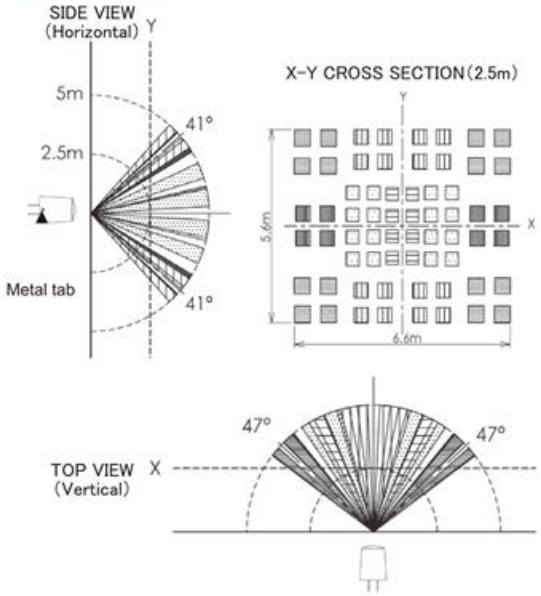

2) Long Distance detection type

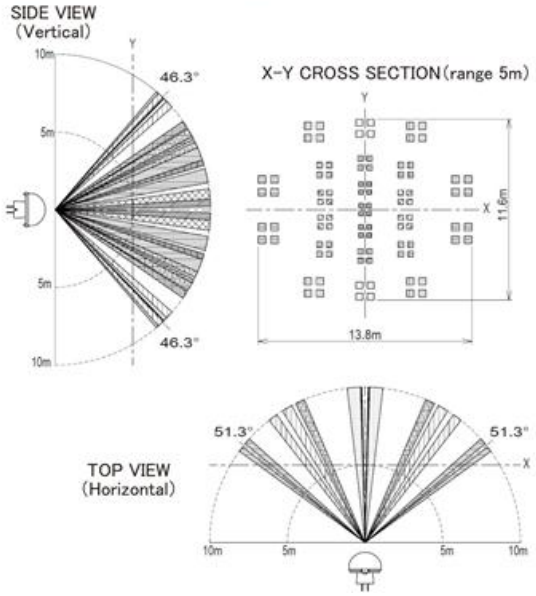

2. Detection Zone Notes

As shown on the diagram, the detection zone is polarized. If a target enters the detection zones + and – at the same time, the signals are respectively cancelled and detection could become impossible at maximum detection range. (Please refer to the detection area diagram for details)

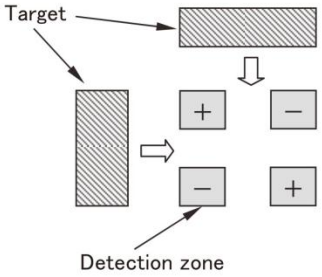

HOW TO USE

1. Wiring Diagram (Digital Output)

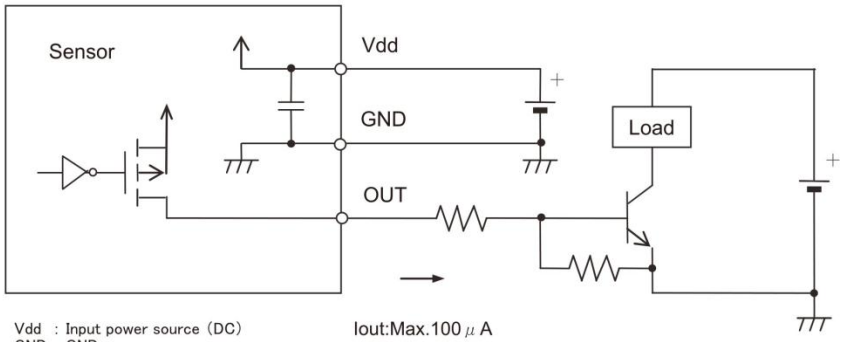

Vdd : Input power source (DC)
GND : GND
Out : Output (Comparator)

Iout:Max.100 μ A

2. Moving Direction

As detailed on the diagram, please install the sensor so that the expected trespassing direction corresponds to the axis X or axis Y.

In some cases, intrusions that occur parallel to the axis Z in every detection zone, closing toward the sensor, may not be detected.

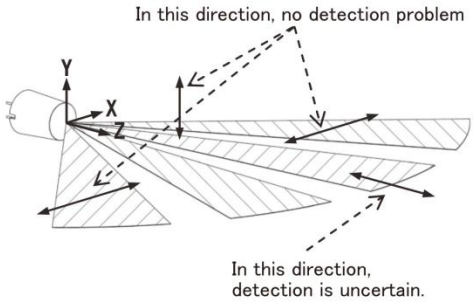

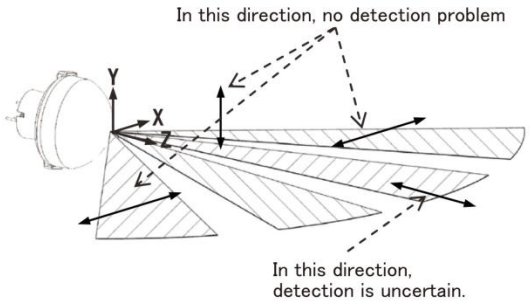

DIMENSION

1) Standard Detection type

A-A Cross Sectional

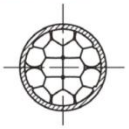

Dimensions

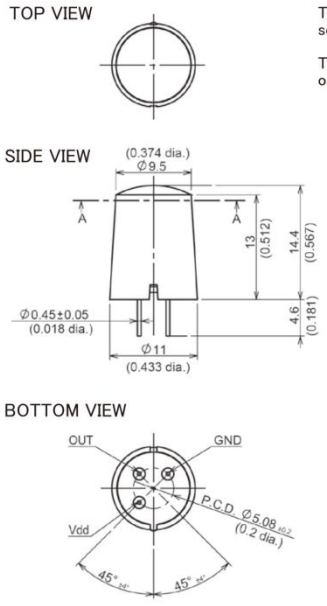

When designing your products

To maintain specified detection capability, position the sensor so that the lens tip is a minimum 1.3mm above the chassis.

The chassis hole requires a taper according to the lens shape, or a larger hole.

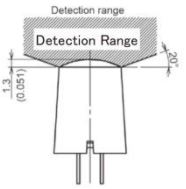

Recommended Hole Drilling Diameter

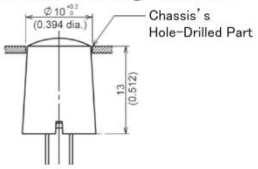

Recommended PCB Pattern Design

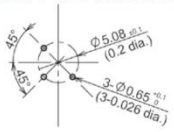

2) Long Distance Detection type

A-A Cross Sectional

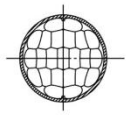

Dimensions

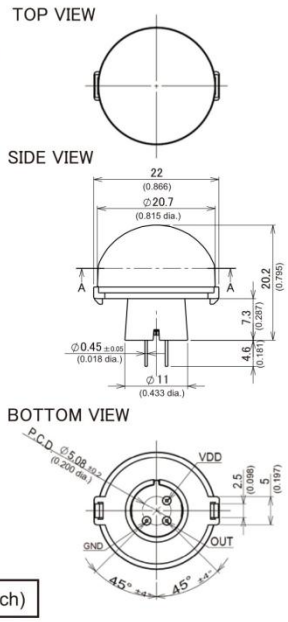

When designing your products

To maintain specified detection capability, please place and expose the sensor so that tip of lens will be more than 7.1mm above the chassis.

The hole of the chassis should have a taper depending on the lens shape, or have a bigger hole.

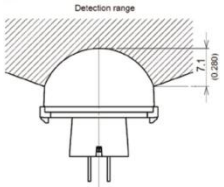

Recommended Hole Drilling Diameter

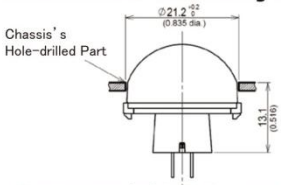

Recommended PCB Pattern Design

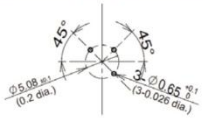

General Tolerance ±0.5mm (±0.020inch)

References

[1] K. Imolauer, R. Pera, S. Bartels and S. Brandes "Market and business chances in the EU in the field of renewable energies and energy efficiency," IEEE, 29th International Telecommunications Energy Conference, INTELEC 2007. pp. 477 - 480.

[2] L. Antonio "Will we exceed 50% efficiency in photovoltaics?," IEEE, 2011, Applied Physics, Vol. 110, pp. 031301 - 031301-19.

[3] K. Zweibel "Should solar photovoltaics be deployed sooner because of long operating life at low, predictable cost?," Elsevier, November 2010, Energy Policy, Vol. 38, pp. 7519–7530.

[4] D. Guru, P. Zhao and Q. Yu "Integration of large wind power plants into power system - challenges and solutions.," IEEE, International Conference on Power System Technology (POWERCON), 2010. p. 1.

[5] S. Ghosh and P.P. Sengupta "Energy Management in the Perspective of Global Environmental Crisis: An Evidence from India," IEEE, International Conference on Management and Service Science (MASS), 2011. pp. 1-5.

[6] S. Mukherjee "Opportunities and challenges with net zero energy buildings," IEEE, 23rd International Symposium on Power Semiconductor Devices and ICs (ISPSD), 2011. pp. 1-5.

[7] M.S. Todorović, O.E. Djurić, I. Matinović and D. Ličina "Renewable energy sources and energy efficiency for building's greening: From traditional village houses via high-rise residential building's BPS and RES powered co- and tri-generation towards net ZEBuildings and Cities,"

IEEE, 3rd International Symposium on Exploitation of Renewable Energy Sources (EXPRES), 2011. pp. 29-37.

[8] Wayne Wolf, Computers as components: principles of embedded computing system design. Burlington, USA: Elsevier, 2008.

[9] R. Foster, M. Ghassemi and A. Cota. Solar energy: renewable energy and the environment. Florida: CRC Press, 2010.

[10] C. Deline “Partially Shaded Operation of a Grid-Tied PV System,” 34th IEEE Photovoltaic Specialists Conference, Philadelphia, PA, 2009.

[11] S. Vergura, G. Acciani, V. Amoruso, G.E. Patrono and F. Vacca "Descriptive and Inferential Statistics for Supervising and Monitoring the Operation of PV Plants," IEEE, 2009, Vol. 56, 11, pp. 4456 - 4464 .

[12] W.N.W. Muhamad, M.Y.M. Zain, N. Wahab, N.H.A. Aziz and R.A. Kadir "Energy Efficient Lighting System Design for Building," IEEE. International Conference on Intelligent Systems, Modelling and Simulation (ISMS), 2010. pp. 282 - 286.

[13] J.J. Cooley, D. Vickery, A.-T. Avestruz, A. Englehart, J. Paris and S.B Leeb "Solid-state lamp with integral occupancy sensor," Twenty-Fifth Annual IEEE Applied Power Electronics Conference and Exposition (APEC), 2010. pp. 2305 - 2313.

[14] M.S. Shur and R. Zukauskas "Solid-State Lighting: Toward Superior Illumination," Proceedings of the IEEE, 2005, Vol. 93, pp. 1691 - 1703.

[15] Jim Geier "Wireless Networks first-step," Cisco Press, 2004.

[16] R. Prasad and Luc Deneire "From WPANs to Personal Networks: Technologies and Applications," Artech House, 2005.

[17] Nick Hunn "Essentials of Short-Range Wireless," Cambridge University Press, 2010.

[18] H. Labiod, H. Afifi and C. De Santis "Wi-Fi, Bluetooth, ZigBee and Wimax," Dordrecht: Springer, 2007.

[19] Wi-Fi Alliance. [Online] http://www.wi-fi.org/.

[20] The official Bluetooth technology info site. [Online] http://www.Bluetooth.com.

[21] The ZigBee Alliance. [Online] http://www.zigbee.org/.

[22] The Z-Wave Alliance. [Online] http://www.z-wavealliance.org.

[23] ANT Alliance. [Online] http://www.thisisant.com.

[24] John Cowley "Communications and Networking," Springer, 2007.

[25] IEEE 802.15.1 standard revision IEEE std. 802.15.1-2005. [Online] http://standards.ieee.org/getieee802/download/802.15.1-2005_part3.pdf.

[26] BLE software stack. [Online] http://www.ti.com/tool/ble-stack.

[27] Bluetooth core specification version 4.0. [Online] http://developer. bluetooth.org/KnowledgeCenter/TechnologyOverview/Documents/Core_SPEC.pdf.

[28] Y. Hu, G. Wang, L. Shan, Z. Yuan and Y. Ouyang "Inter-piconet interference mitigation schemes for converged BTLE and cellular network," IEEE, 2011, Wireless Communications and Signal Processing.

[29] F. Shahin "ZigBee wireless networks and transceivers," Oxford, UK: Elsevier, 2008.

[30] S. Silvestre and A. Chouder "Shading effects in characteristic parameters of PV modules," IEEE, Spanish Conference on Electron Devices, 2007. pp. 116-118.

[31] C.B. Yahya "Performance monitoring of solar photovoltaic systems using reference cells," ICM 2008. International Conference on Microelectronics, 2008, Sharjah. pp. 445 - 449.

[32] TI CC2530 SoC. [Online] http://www.ti.com/product/cc2530.

[33] CC2530 Evaluation Module. [Online] http://www.ti.com/tool/cc2530emk.

[34] SmartRF05 EB. [Online] http://www.ti.com/lit/ug/swru210a/swru210a.pdf.

[35] SoC-BB. [Online] http://focus.ti.com/lit/ug/swru241/swru241.pdf.

[36] MAX4081. [Online] http://datasheets.maxim-ic.com/en/ds/MAX4080-MAX4081.pdf.

[37] MAX5033 . [Online] http://datasheets.maxim-ic.com/en/ds/MAX5033.pdf.

[38] V. Garg and N.K. Bansal "Smart occupancy sensors to reduce energy consumption," Energy and Buildings, Elsevier, June 2000, Vol. 32, Issue 1, pp. 81-87.

[39] X. Cao , W. Yan , S. Y. Hui and H. S.-H. Chung "Dimming control and characteristics of high-frequency operated metal halide lamps", IEEE Transactions on Power Electronics, 2004, Vol. 19, No. 3, pp. 845-861.

[40] Danny H.W. Li, Joseph C. Lam, "Evaluation of lighting performance in office buildings with daylighting controls," Energy and Buildings, Elsevier, Oct. 2001, Vol. 33, Issue 8, pp. 793-803.

[41] J.D. Jennings, F.M. Rubinstein, D. Dibartolomeo and S.L Blanc "Comparison of control options in private offices in an advanced controls testbed," Journal of the Illuminating Engineering Society, 2000, 29(2):39-60.

[42] S. Matta "An intelligent light control system for power saving," IECON 2010 - 36th Annual IEEE Conference on Industrial Electronics Society, 2010 Glendale, AZ, pp. 3316-3321.

[43] J. Lu et al. "Using simple light sensors to achieve smart daylight harvesting," presented at the Proceedings of the 2nd ACM workshop on embedded sensing systems for energy-efficiency building, 2010 Zurich, switzerland.

[44] Yin Jun and Wang Wei "LED lighting control system based on the ZigBee wireless network," International Conference on Digital Manufacturing and Automation (ICDMA), 2010, ChangSha, China, pp. 892-895.

[45] Dae-Man Han and Jae-Hyun Lim "Smart home energy management system using IEEE 802.15.4 and ZigBee," IEEE Transactions on Consumer Electronics, 2010.

[46] Y. Wang and Zh. Wang "Design of intelligent residential lighting control system based on ZigBee wireless sensor network and fuzzy controller," International Conference on Machine Vision and Human-Machine Interface (MVHI), 2010, Kaifeng, China, pp. 561-564.

[47] W. Guo, W. M. Healy and M. Zhou "Interference impacts on ZigBee-based Wireless Mesh Networks for building automation and control," IEEE International Conference on Systems, Man, and Cybernetics (SMC), 2011, Anchorage, AK, pp. 3452-3457.

[48] S.Y. Shin and S. Choi " Packet error rate analysis of ZigBee under WLAN and Bluetooth interferences," IEEE Transaction on Wireless Communications, 2007, Vol. 6, Issue 8, pp. 2825 - 2830.

[49] T. Mangir, L. Sarakbi and H. Younan "Analyzing the impact of Wi-Fi interference on ZigBee networks based on real time experiments," International Journal of Distributed and Parallel Systems (IJDPS), 2011, Vol. 2, No.4.

[50] Seung-Hwan Lee and Yong-Hwan Lee "Adaptive frequency hopping for Bluetooth robust to WLAN interface," IEEE, 2009, Communications Letters, Vol. 13, pp. 628-630.

[51] TI CC2540. [Online] http://www.ti.com/product/cc2540.

[52] SFH3310 phototransistor. [Online] http://catalog.osram-os.com/catalogue/catalogue.do?favOid=000000020001eab3001d0023&act=showBookmark.

[53] PIR sensor. [Online] http://pewa.panasonic.com/assets/pcsd/catalog/papirs-ekmb-catalog.pdf.

[54] IRFP260 MOSFET. [Online] http://www.irf.com/product-info/datasheets/data/irfp260.pdf.

[55] S. B. Kjaer, J. K. Pedersen and F. Blaabjerg "A review of single-phase grid-connected inverters for photovoltaic modules," IEEE Transactions on Industry Applications, 2005, Volume 41, Issue 5, pp. 1292-1306

[56] H. Patel and V. Agarwal "MPPT scheme for a PV-fed single-phase single-stage grid-connected inverter operating in CCM with only one current sensor", IEEE Transactions on Energy Conversion, Volume 24, Issue 1, pp. 256-263, March 2009.

[57] W. Nianchun, X. Quingshan, Sh. Bin, K. Yukita, Y. Goto and K. Ichiyanagi "Research of single-phase inverter for PV modules with MPPT," APPEEC Power and Energy Engineering Conference, 2009, Asia-Pacific. pp. 1-4.

[58] Carlos A. P. Tavares, Karla T. F. Leite, Walter I. Suemitsu and Maria D. Bellar “Performance evaluation of photovoltaic solar system with different MPPT methods," 35th Annual Conference of IEEE on Industrial Electronics, IECON '09. 2009, Porto, pp. 719-724.

[59] G. Gupta, D. Kastwar, A. Hussain and H. Ranjan “Modeling and design of MPPT controller for a PV module using PSCAD/EMTDC," IEEE PES Innovative Smart Grid Technologies Conference Europe (ISGT Europe), 2010, Gothenburg. pp. 1-6.